Measurement of the Higgs boson in decays to bosons using the ATLAS detector

Dongshuo Du

University of Science and Technology of China

2022.08.09

中国物理学会高能物理分会第十一届全国会员代表大会暨学术年会
辽宁师范大学, 2022/08/08 -2022/08/11

Outline

- Overview of Higgs physics in diboson final states

- Higgs boson cross sections measurement
  - Measurement of Simplified Template Cross Section (STXS) in $H \rightarrow WW^*$, $H \rightarrow ZZ^*$ and $H \rightarrow \gamma\gamma$ decay channels
  - Fiducial inclusive and differential cross-section measurements in $H \rightarrow ZZ^*$ and $H \rightarrow \gamma\gamma$ decay channels

- Summary

Higgs Physics In Diboson Final States

- The most prolific decay: H →bb (58%), very hard to observe

- The branching ratios (BR) of H → WW*(→lvlv) /γγ/ ZZ*(→4l) are 1.0%, 0.23% and 0.012%, respectively

- The final states (e, μ, γ) are very sensitive & leave a clean signature in the ATLAS detector
  - H→ZZ*→4l and H →γγ : the most sensitive channels for observation
    - H→ZZ*→4l, S/B > 2
    - H→γγ, S/B ~5%
  - H→ WW*→lvlv (high yield with fair S/B)
    - Larger branching ratio
    - Clean signature
    - High background

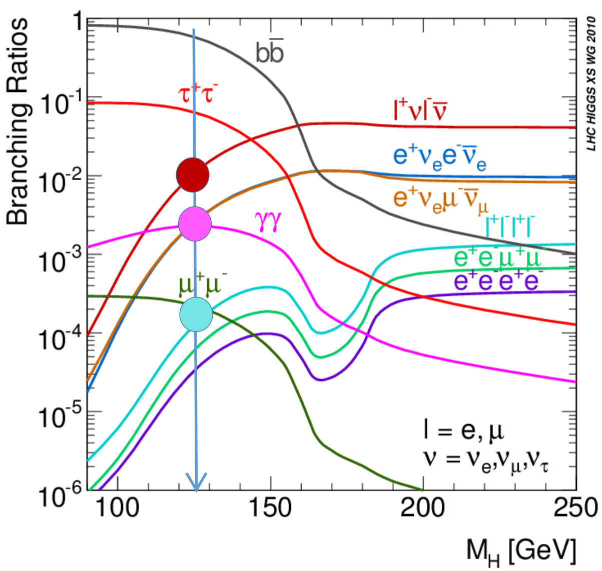

⟹ Powerful tool for measuring the Higgs properties

Simplified Template Cross Section (STXS)

- The aim with STXS method:
  - Improve sensitivity of measurements
  - Reduce their dependence on the theory
  - Isolation of possible BSM effects

- STXS framework provides different stages (e.g. stage 0, stage 1, stage 1.2) with increasingly fine granularity, [more details]()

- Categorizing events into bins of key (truth) variables (p_T^H, N_{jets}, m_{jj}) in different production modes (ggH, qqH, VH and ttH)

- STXS well-suited to combine different decay channels

- Higgs boson properties measured with 139 fb^{-1} ($\sqrt{s}$ = 13 TeV) for Higgs boson rapidity $|y_H| < 2.5$

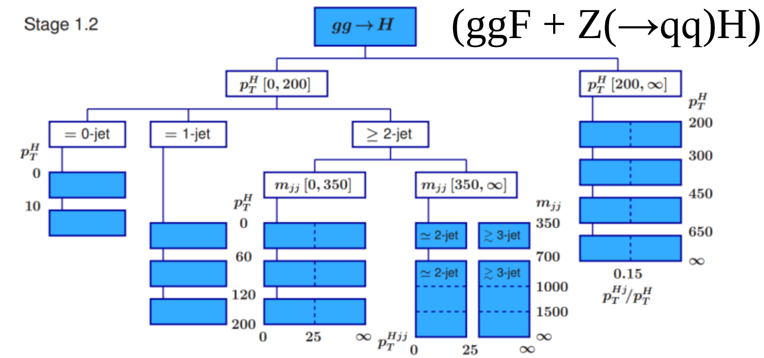

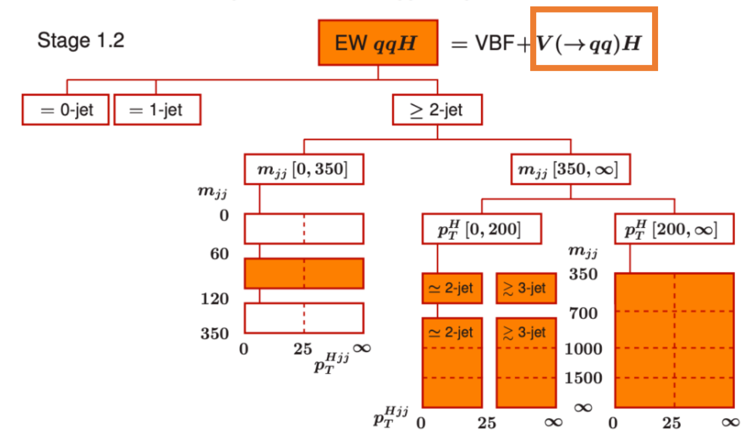

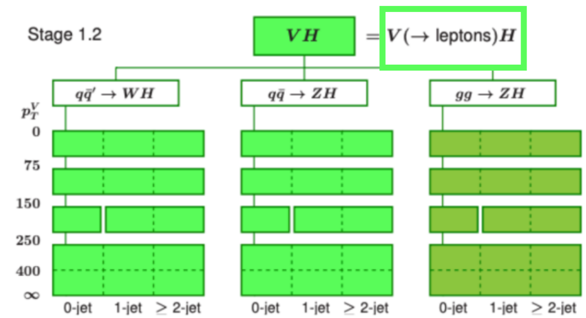

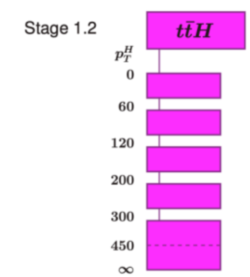

H→WW*: Analysis Strategy

- Signal: different flavour (eμ+μe) opposite charge leptons + MET

Submitted to PRD

- Events split in 4 analysis categories based on N_{jets} (*)
  - ggF: $N_{jets} = 0, 1, \geq 2$, cut based
    - m_T used as discriminant variable
  - VBF: $N_{jets} \geq 2$, "deep" neural network (DNN) based
    - DNN used as discriminant variable

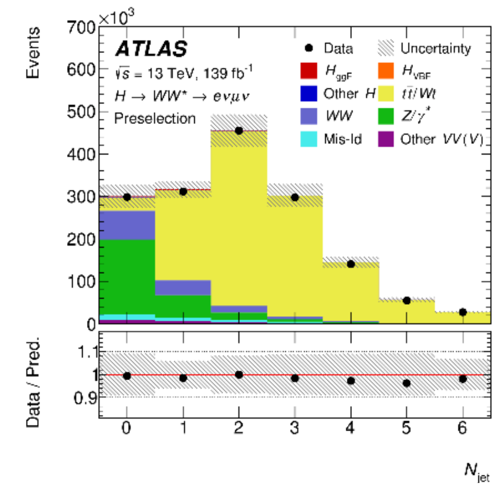

- Main background:
  - Non-resonant qqWW, top and Z→ττ
    - ggF: qqWW, top and Z→ττ normalized by control regions (CR)
    - VBF: top and Z→ττ normalized by CRs
  - Background with mis-identified leptons estimated by data-driven fake factor method

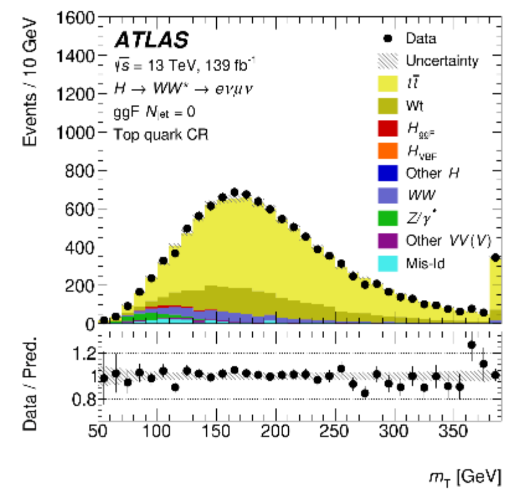

(*) Full event selection in the backup

$$m_T = \sqrt{(E_T^{\ell\ell} + E_T^{\text{miss}})^2 - |\mathbf{p}_T^{\ell\ell} + \mathbf{E}_T^{\text{miss}}|^2}, \quad E_T^{\ell\ell} = \sqrt{|\mathbf{p}_T^{\ell\ell}|^2 + m_{\ell\ell}^2}$$

H→WW*: STXS

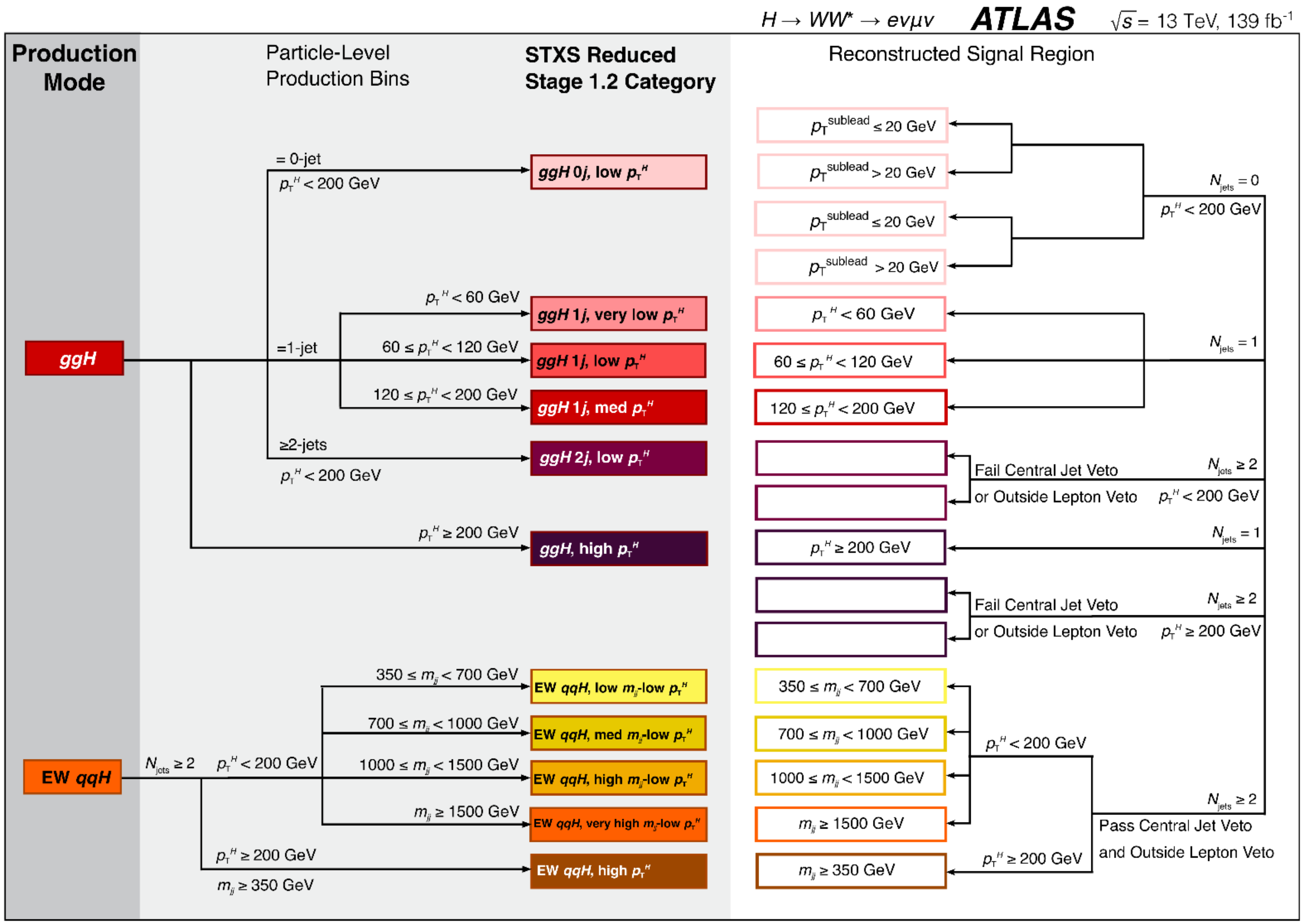

[Submitted to PRD]

- Split by p_T^H, N_{jets}, m_{jj} into 11 categories
- 17 signal regions (SR)
- 27 control regions (CR)

- This analysis based on the reduced stage 1.2 category to ensure sensitivity for all measurements.
- CRs split similar to SRs where statistics allow

$$p_T^H = |\boldsymbol{p}_T^{\ell\ell} + \boldsymbol{E}_T^{\text{miss}}|$$

H→WW*: Results

Submitted to PRD

Coupling results

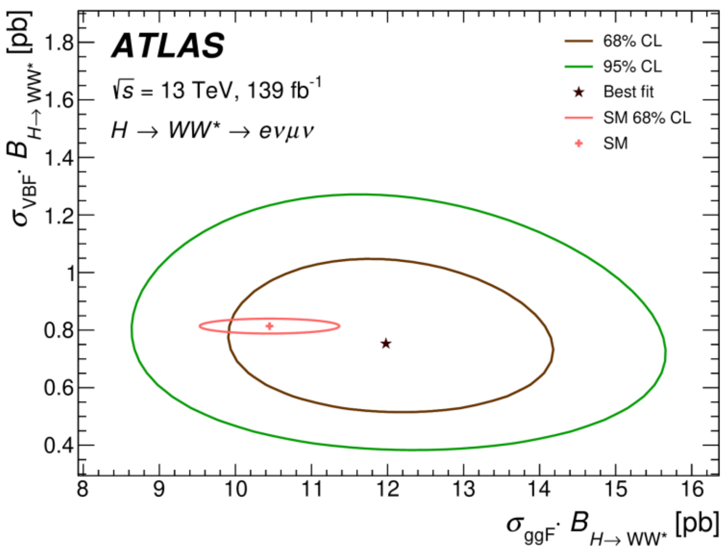

STXS results

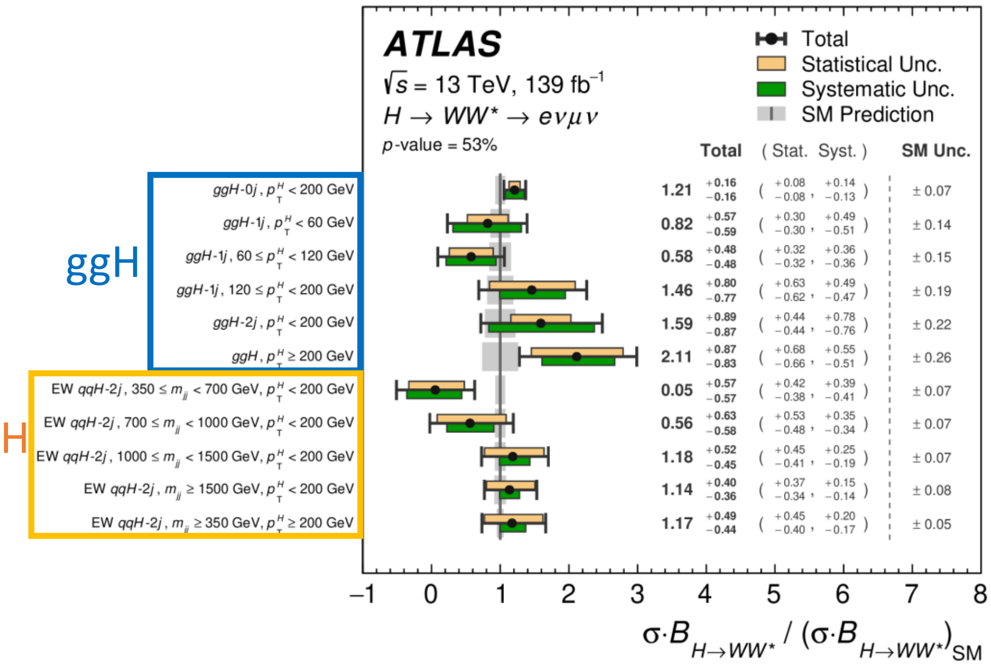

$$\boxed{\sigma_{\mathrm{ggF}} \cdot \mathcal{B}_{H\to WW^*} = 12.0 \pm 1.4\ \mathrm{pb}}$$
$$= 12.0 \pm 0.6\ (\mathrm{stat.})\ ^{+0.9}_{-0.8}\ (\mathrm{exp.\ syst.})\ ^{+0.6}_{-0.5}\ (\mathrm{sig.\ theo.})\ \pm 0.8\ (\mathrm{bkg.\ theo.})\ \mathrm{pb}$$
$$\boxed{\sigma_{\mathrm{VBF}} \cdot \mathcal{B}_{H\to WW^*} = 0.75\ ^{+0.19}_{-0.16}\ \mathrm{pb}}$$
$$= 0.75 \pm 0.11\ (\mathrm{stat.})\ ^{+0.07}_{-0.06}\ (\mathrm{exp.\ syst.})\ ^{+0.12}_{-0.08}\ (\mathrm{sig.\ theo.})\ ^{+0.07}_{-0.06}\ (\mathrm{bkg.\ theo.})\ \mathrm{pb},$$

- Compatible with SM predictions within 1 σ

- Extracted by profile likelihood fit: 17 SRs (m_T/DNN) + 27 CRs
- ggH uncertainties limited by both stat. + syst. uncertainty
- qqH uncertainties limited by statistical uncertainty at high m_{jj} / p_T^H

H→ZZ*→4ℓ: Four-lepton Invariant Mass Distribution

Analysis features：

- **Small branching fraction (0.0124% at m_H = 125 GeV)**
- **Best final S/B ratio, better than 2:1**
- **Clean signature with fully reconstructed final state**
- **good mass resolution = 1-2%**

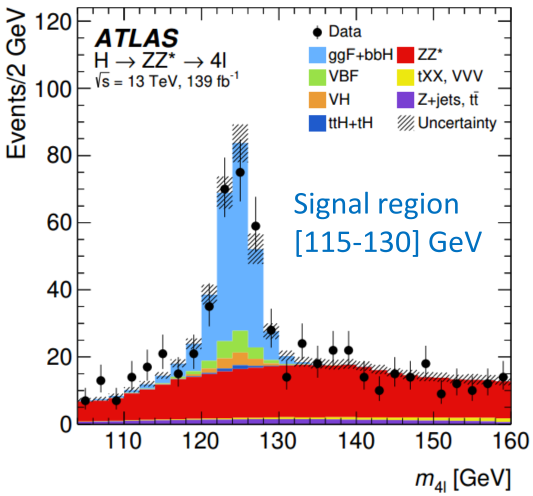

Eur. Phys. J. C 80, 957 (2020).

Signal: 4 leptons (4e, 4μ, 2e2μ and 2μ2e)

Backgrounds:

- Dominant background: Non-resonant ZZ*/Zγ*, estimated from data sideband (105–160 GeV)
- Reducible background with non-prompt leptons for Z+jets, ttbar constrained by dedicated CR.

Cross sections extracted by fit to the NN observable

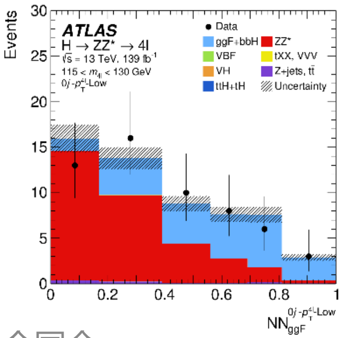

ggF 0jet category with $p_T^H < 10$ GeV

H→ZZ*→4ℓ: STXS

Eur. Phys. J. C 80, 957 (2020).

Production Mode Stage

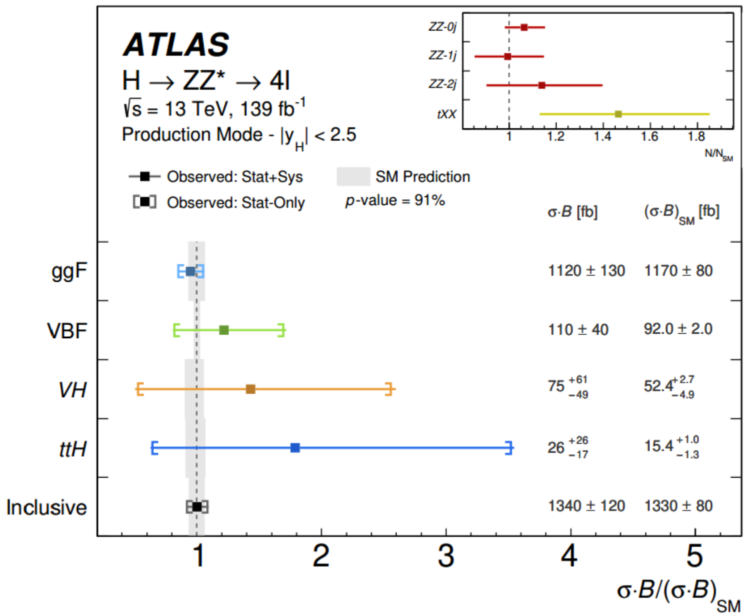

Reduced Stage 1.1

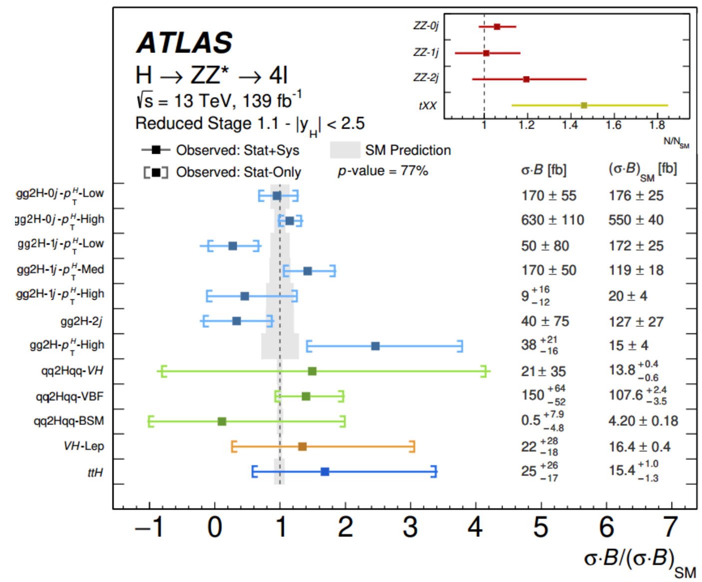

- The inclusive H→ZZ* production cross-section for $|y_H| < 2.5$:
  1.34 ± 0.12 pb
- Good agreement with the SM predictions:
  1.33 ± 0.08 pb
- 12 pois measured simultaneous
  - ggF/VBF: 7/3 categories separately
  - VH-lep/ttH: One bin from each mode
- Due to finer categorization, results are statistically limited.

H→γγ: Diphoton Invariant Mass Distribution

[Submitted to JHEP]

Analysis features:

- Fairly high branching fraction **wrt** H→ZZ*→4ℓ: **~20 times larger**
- **Excellent performance of photon reconstruction and identification**
- **Final states are fully reconstructable**
- **Good mass resolution = 1-2%**

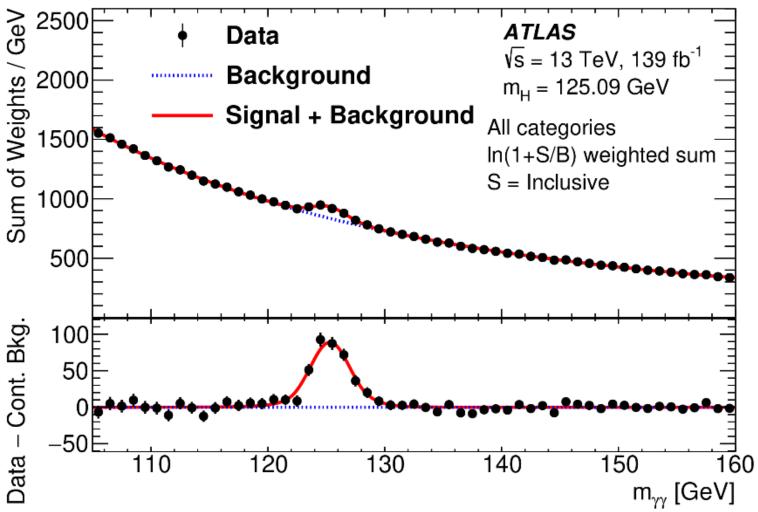

Signal + background model fit for all categories with $m_{\gamma\gamma}$, and the residual plot after subtracting the backgrounds

Signal: diphoton

Backgrounds:

- SM diphoton production (>75%) or γ+jets (~20%), jet+jets (<5%) estimated from data sideband

H→γγ: Production Mode Cross Sections

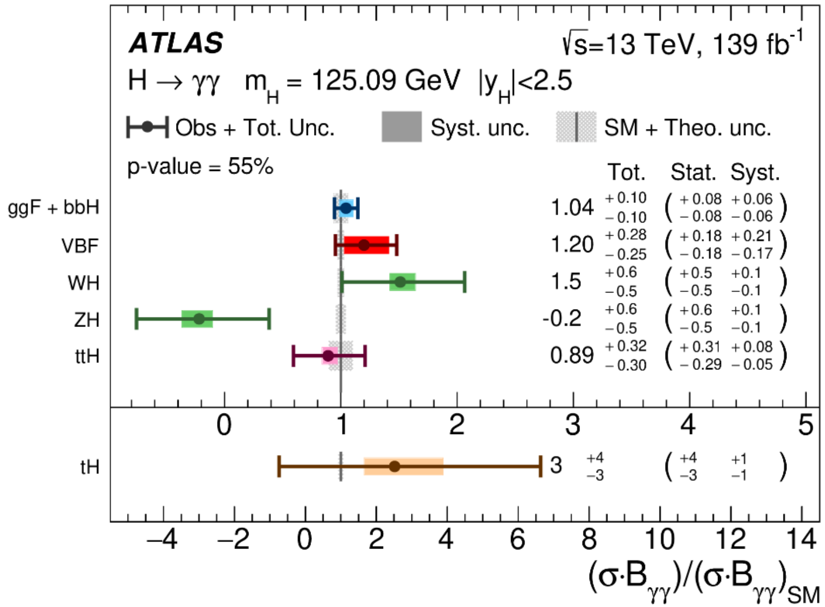

Process ($\lvert y_H \rvert < 2.5$)	Value [fb]	Uncertainty [fb] Total	Stat.	Syst.	SM pred. [fb]
ggF+$b\bar{b}H$	106	$^{+10}_{-10}$	$^{+8}_{-8}$	$^{+6}_{-6}$	102^{+6}_{-6}
VBF	9.5	$^{+2.2}_{-1.9}$	$^{+1.5}_{-1.4}$	$^{+1.7}_{-1.4}$	$7.9^{+0.2}_{-0.2}$
WH	4.2	$^{+1.5}_{-1.4}$	$^{+1.5}_{-1.4}$	$^{+0.4}_{-0.2}$	$2.8^{+0.1}_{-0.1}$
ZH	−0.4	$^{+1.1}_{-1.0}$	$^{+1.1}_{-1.0}$	$^{+0.2}_{-0.3}$	$1.8^{+0.1}_{-0.1}$
$t\bar{t}H$	1.0	$^{+0.4}_{-0.3}$	$^{+0.3}_{-0.3}$	$^{+0.1}_{-0.1}$	$1.1^{+0.1}_{-0.1}$
tH	0.5	$^{+0.8}_{-0.6}$	$^{+0.7}_{-0.6}$	$^{+0.3}_{-0.2}$	$0.19^{+0.01}_{-0.02}$

Submitted to JHEP

- The contribution from the bbH process is included in the ggF
- Good agreement with SM prediction.
- $\sigma_{tH}^{Obs\ (exp)}$ < 10 (6.8) σ_{tH}^{SM} at 95% CL
  - Unique sensitivity to the sign of the top-quark Yukawa coupling

- The overall Higgs boson signal strength:

$$\mu = 1.04^{+0.10}_{-0.09} = 1.04 \pm 0.06\ (\text{stat.})^{+0.06}_{-0.05}\ (\text{theory syst.})\ ^{+0.05}_{-0.04}\ (\text{exp. syst.}).$$

Good agreement with SM prediction

H→γγ: STXS

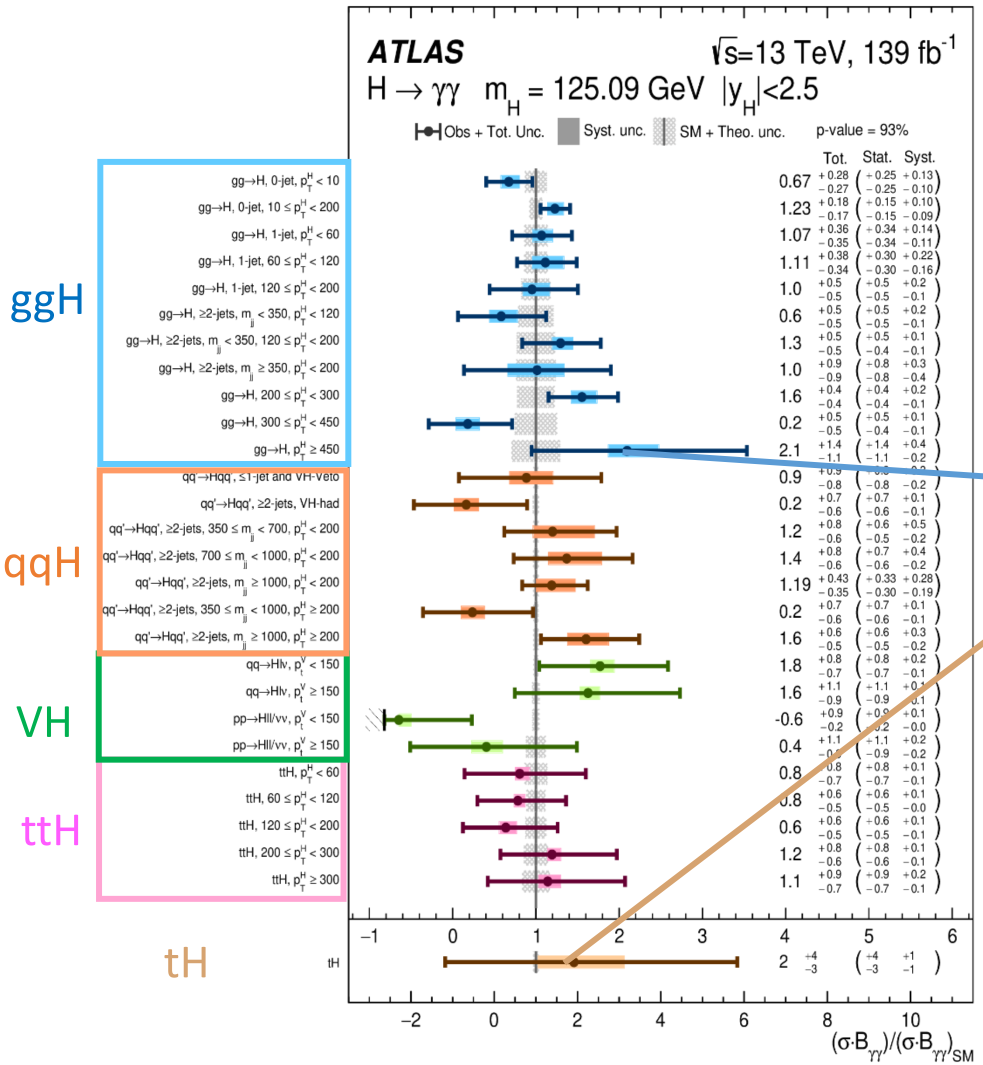

[Submitted to JHEP]

- More statistics with Full Run2 dataset, finer binning especially for non-ggH production mode.
- Cross-sections of 28 STXS regions are measured
  - First to measure ttH differentially
  - Access to the very high p_T^H region
  - Access to tH production mode ($tHqb$ and tHW)
- Very good agreement with SM prediction with a p-value of 93%.
- Due to finer categorization, measurements are statistically limited.

Differential and Fiducial Cross Sections

- Fiducial region: The fiducial selection closely match the detector level
  - Minimise model-dependent acceptance extrapolations
  - Allow for easy comparison of physics models today and in the future

$$\sigma^{\text{fid}} = \sigma^{Total} \times A \times BR = \frac{N_s}{C \times L_{\text{int}}}$$

N_s : number of observed signal events, $C = \frac{N_{\mathrm{Re}\,c}}{N_{Fid}}$: the correction factor for detector efficiency and resolution effect, L_{int} : Integrated luminosity

- Inclusive fiducial cross-section: No attempt to separate Higgs production/decay modes → compare with best available predictions in the detector phase space

- Differential cross-section: Different differential cross-section measurement sensitive to the different physics:
  - The Higgs p_T distribution can test couplings to b and c quarks, and high p_T can tests new physics.
  - The jet multiplicity is sensitive to different production mechanisms and the theoretical modelling of high-quark and gluon emission.

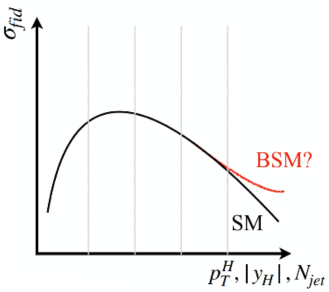

- Combination needs extrapolation to the full phase space due to the fiducial regions are different (acceptance + BR)

H→ZZ*→4ℓ: Inclusive and Differential Cross Section

Eur. Phys. J. C 80, 942 (2020)

- H→ZZ*→4ℓ decay mode provides excellent resolution for Higgs kinematic variables
- Fitting 4ℓ distribution in each final state (right) or **differential bin** (bottom)to extract the measured cross section

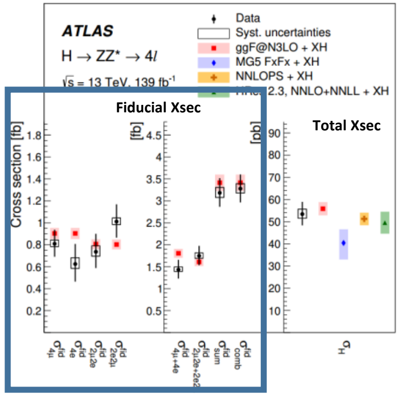

Inclusive fiducial cross section:

$$\sigma_{\mathrm{fid}} = 3.28 \pm 0.30\ (\mathrm{stat.}) \pm 0.11\ (\mathrm{syst.})\ \mathrm{fb}$$
$$\sigma_{\mathrm{fid},SM} = 3.41 \pm 0.18\ \mathrm{fb}$$

10% level precision and Good agreement with LHCXSWG prediction

Differential cross section with 20 observables:

- 9 Higgs kinematic-related variables: like p_T^H
- 7 Jet-related variables: like N_{jets}
- 4 Higgs boson and jet-related variables

Measured cross sections in good agreement with SM predictions within uncertainties

Limited by statistical uncertainties

Low p_T^H test couplings to b and c quarks and High p_T^H test BSM

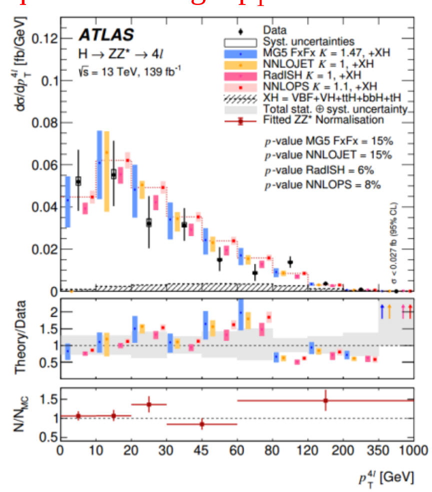

Sensitive to production mode

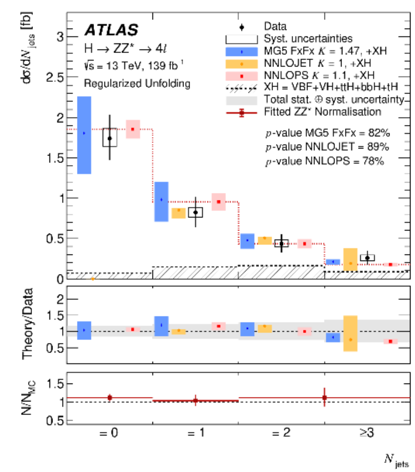

Predictions for comparison

H→γγ: Inclusive and Differential Cross Section

- Excellent performance of photon reconstruction and identification
  → **good resolution for Higgs variables**
- The H → γγ signal yields are extracted from fits to the diphoton invariant mass spectrum

Inclusive fiducial cross section:

$$\sigma_{\text{fid}} = 67 \pm 6 \text{ fb}$$

$$\sigma_{\text{fid},SM} = 64.2 \pm 3.4 \text{ fb}$$

The measurement has precision at 9% level

Differential cross-section still limited by statistical uncertainties

Low p_T^H test couplings to b and c quarks and High p_T^H test BSM

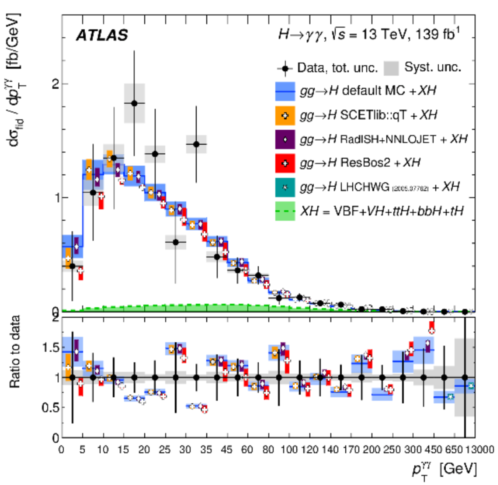

N_{jets} → test modelling of radiations at high pT and production modes

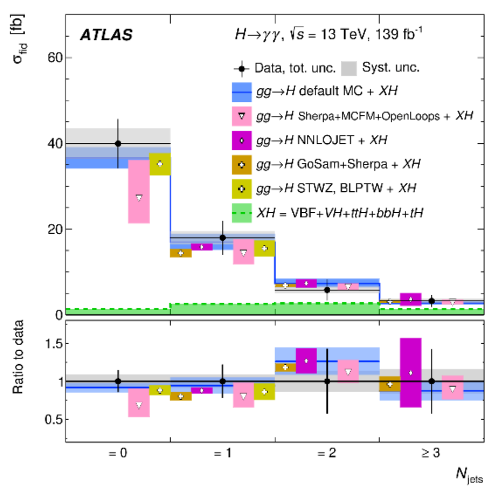

Double-differential cross section: $p_T^{\gamma\gamma}$ in bins of $|y_{\gamma\gamma}|$

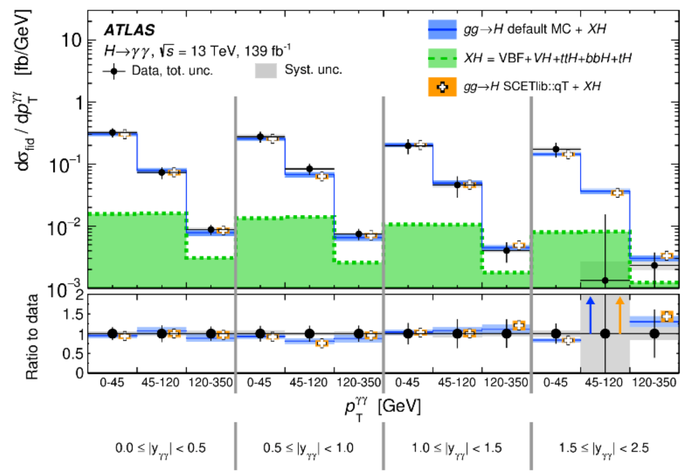

Measured cross sections in good agreement with SM predictions within uncertainties

[Accepted by JHEP](#)

[More details in Fabio's talk](#)

Combination: H → γγ and H → ZZ

- Combination between H → γγ and H → ZZ can improve the measurement precision.
  - Based on the individual channel
  - The uncertainties from same source are correlated
  - Both channels are extrapolated to the full phase space to do the combination

- The Combined differential result still dominated by the statistical uncertainty

Submitted to JHEP

Measured total XS: $55.5^{+4.0}_{-3.8}$ pb
SM prediction: 55.6 ± 2.8 pb

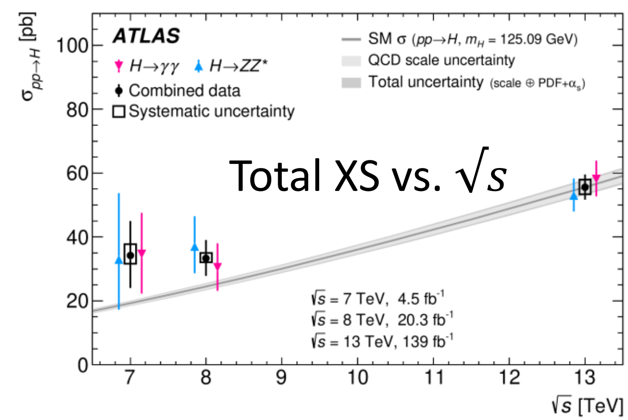

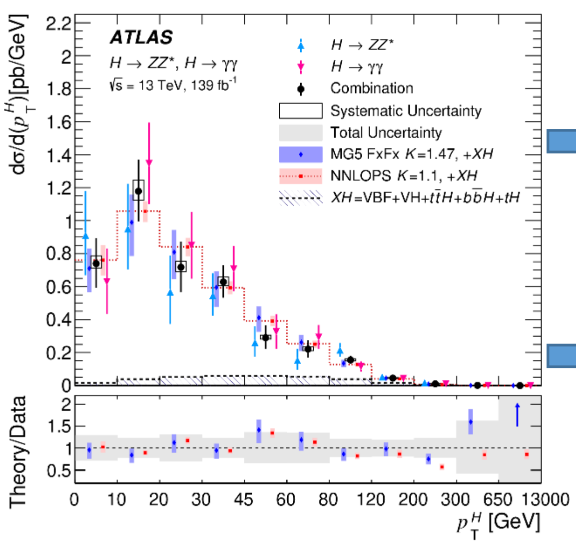

p_T^H precision:
20-30% up to 300 GeV
~60% 300-650 GeV
>100% 650-1200 GeV

With more date, the precision can be further improved

The differential XS distribution of p_T^H can used to indirect constrain the Yukawa coupling of charm and bottom quark (k_c and k_b).

More details in Tao's talk

Summary

- $H \rightarrow ZZ^*$, $H \rightarrow \gamma\gamma$, $H \rightarrow WW^*$ channels investigated with 139 fb^{-1} of data collected with the ATLAS detector @13TeV
  - Inclusive, STXS and differential cross section measurements are presented
  - All the measurements are in agreement with the SM predictions
  - The precision of the fiducial cross section measurement in both $H \rightarrow ZZ^*$ and $H \rightarrow \gamma\gamma$ channel about 10%.
  - All the differential cross section measurement still dominant by the statistical uncertainty
- **Run3 has just started with much more to come. Stay tuned!**

Thank you for your attention

Back up

Higgs Physics In Diboson Final States

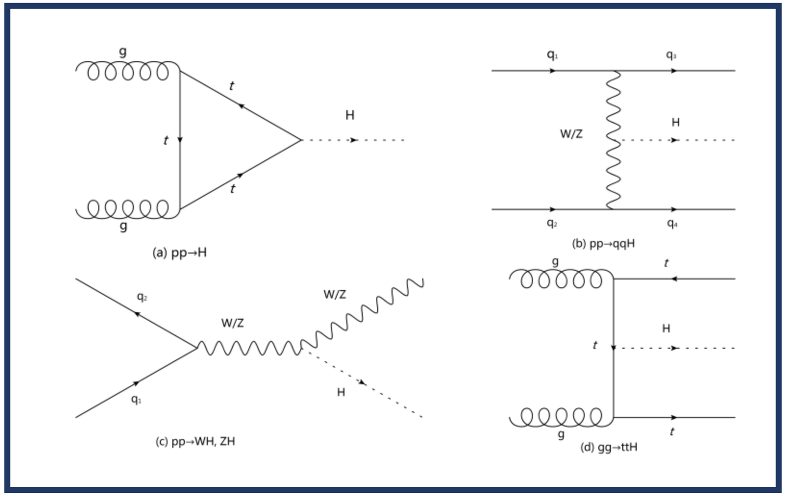

Production modes

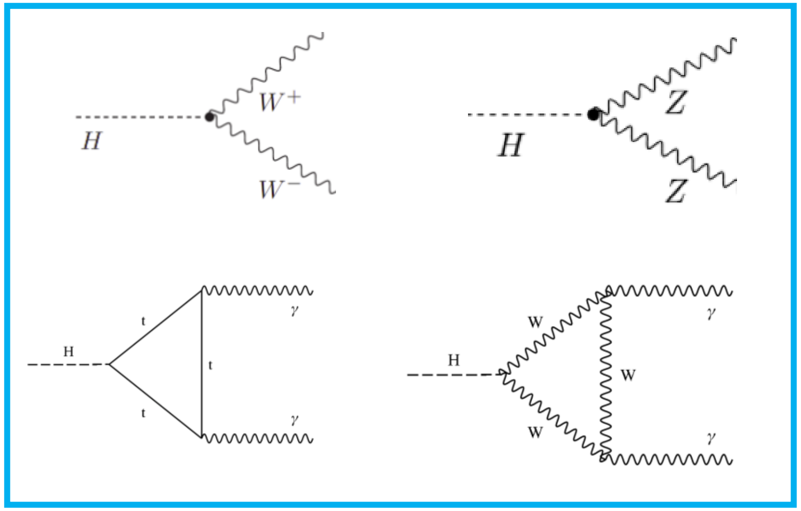

Higgs decay to diboson

- The most prolific decay: H →bb (58%), very hard to observe
- The branching ratios (BR) of H → WW*(→lvlv) /ZZ*(→4l)/γγ are 1.0%, 0.012% and 0.23%, respectively
- The final states (e, μ, γ) are very sensitive & leave a clean signature in the ATLAS detector

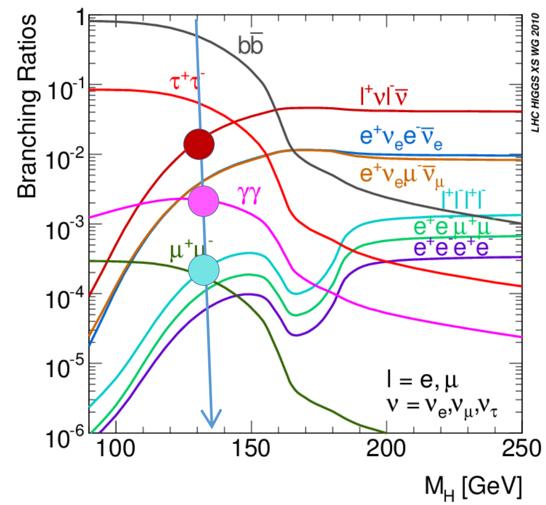

Higgs mass measurement

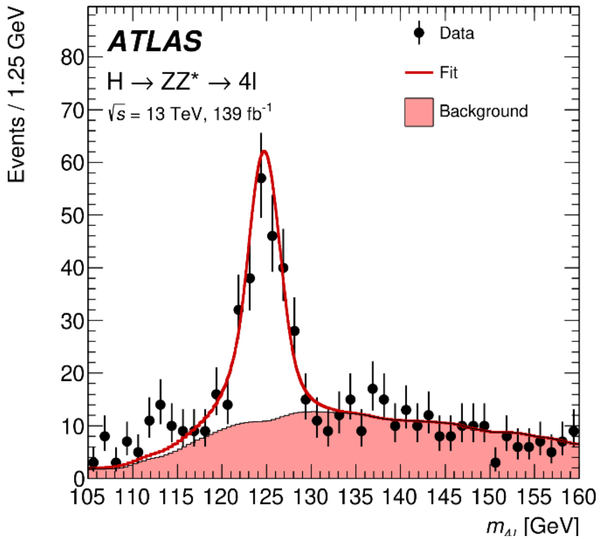

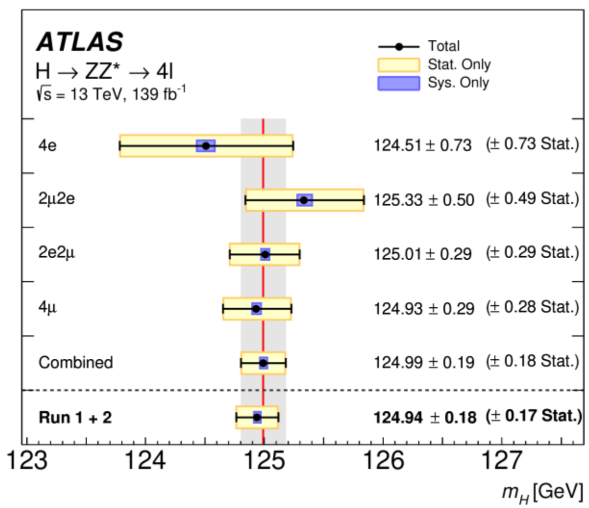

Submitted to Physics Letters B

- First mass measurement of Higgs boson with HZZ channel by using Full Run2 data

$$m_H = 124.99 \pm 0.18(\text{stat.}) \pm 0.04(\text{syst.})\ \text{GeV}.$$

- m_H is extracted by performing a simultaneous fit to the four subchannels (4μ, $2e2\mu$, $2\mu 2e$, and $4e$) in the $m_{4\ell}$ range between 105 and 160 GeV.
- The results are still limited by statistical uncertainty
- Run1+Run2 combined results with new correlation scheme(Systematic uncertainties largely reduced)

$$m_H = 124.94 \pm 0.17(\text{stat.}) \pm 0.03(\text{syst.})\ \text{GeV},$$

- The most precise measurement of m_H in the $H \to Z Z* \to 4\ell$ channel by the ATLAS Collaboration

More details in Han Li's talk

More about the Fiducial and differential cross sections measurement

Fiducial region is defined to closely match to experimental acceptance

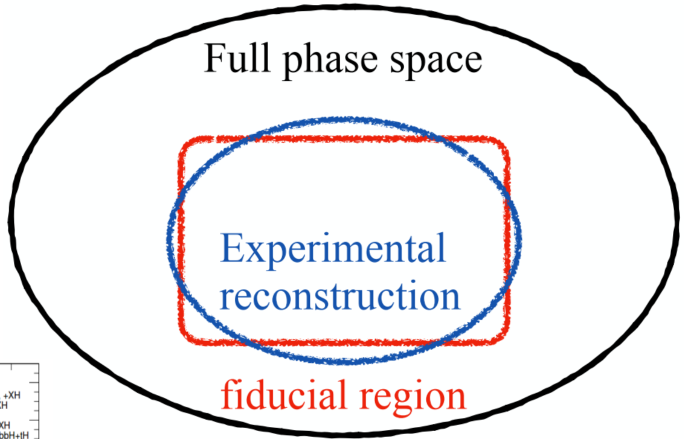

To obtain the data distributions in fiducial region, the response matrix R_{truth_reco} is used to accounting for the bin migrations

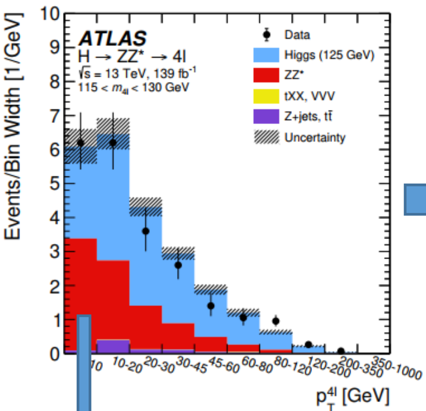

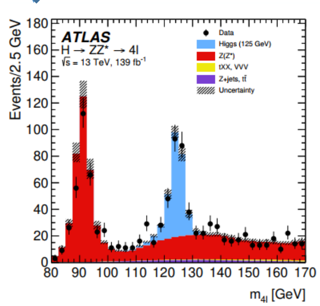

Unfolding

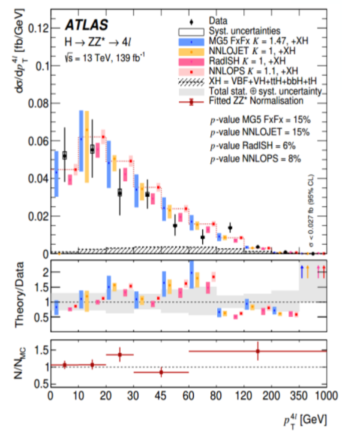

$$N_r^{(H)} = \frac{1}{C_r^{\mathrm{fid}}} \left[\sum_t L \times (\sigma_t \times B_{\gamma\gamma}) \times R_{t,r} \right],$$

C_r^{fid}: Corrects for events that pass selection but outside of the fiducial region.

$R_{t,r}$ is the response matrix.

Response Matrix: few percent migration

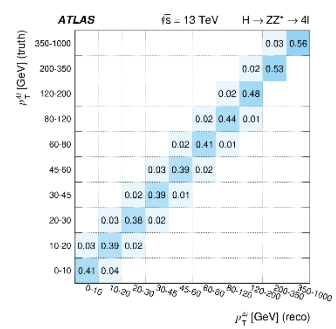

Main improvement for HWW analysis

Big picture:

1. Total integrated luminosity
2. Additional consider ggF 2jet analysis
3. STXS also measured in this analysis

More specific:

① Ttbar nnlo reweighting to correct the mismodeling ofthe leading-lepton P_T due to missing higher-order corrections
② B-tagging change from MV2C10 to DL1r
③ DNN to replace the BDT for VBF analysis
④ The central jet veto is applied for jets with pT > 30 GeV, compared to pT > 20 GeV used previously, reducing the theory modelling uncertainty

…

Main improvement for H γγ

- New categorization; ～20% improvement in sensitivity.
- Increased granularity; 28 STXS categories from 101 reconstruction categories

Categorization

The previous analyses performed such categorization sequentially, giving higher priority to production processes with lower cross sections, the new strategy considers all production processes simultaneously.

1. Signal multi-class BDT: splits signal into STXS regions, aiming to simultaneously reduce the uncertainties and correlations between the classes.
2. Background rejection binary BDT: in each of the signal multi-class BDT output classes a dedicated BDT is trained. This BDT aims to separate signal from the backgrounds.

Multi-class BDT: Training variables

Submitted to JHEP

η_{γ_1}, η_{γ_2}, $p_{\mathrm{T}}^{\gamma\gamma}$, $y_{\gamma\gamma}$,
$p_{\mathrm{T},jj}^{\dagger}$, m_{jj}, and Δy, $\Delta\phi$, $\Delta\eta$ between j_1 and j_2,
$p_{\mathrm{T},\gamma\gamma j_1}$, $m_{\gamma\gamma j_1}$, $p_{\mathrm{T},\gamma\gamma jj}{}^{\dagger}$, $m_{\gamma\gamma jj}$
Δy, $\Delta\phi$ between the $\gamma\gamma$ and jj systems,
minimum ΔR between jets and photons,
invariant mass of the system comprising all jets in the event,
dilepton p_{T}, di-e or di-μ invariant mass (leptons are required to be oppositely charged),
$E_{\mathrm{T}}^{\mathrm{miss}}$, p_{T} and transverse mass of the lepton + $E_{\mathrm{T}}^{\mathrm{miss}}$ system,
p_{T}, η, ϕ of top-quark candidates, $m_{t_1 t_2}$
Number of jets†, of central jets ($|\eta| < 2.5$)†, of b-jets† and of leptons,
p_{T} of the highest-p_{T} jet, scalar sum of the p_{T} of all jets,
scalar sum of the transverse energies of all particles ($\sum E_{\mathrm{T}}$), $E_{\mathrm{T}}^{\mathrm{miss}}$ significance,
$\left|E_{\mathrm{T}}^{\mathrm{miss}} - E_{\mathrm{T}}^{\mathrm{miss}}(\text{primary vertex with the highest } \sum p_{\mathrm{T,track}}^2)\right| > 30\,\mathrm{GeV}$
Top reconstruction BDT of the top-quark candidates,
$\Delta R(W, b)$ of t_2,
η_{j_F}, $m_{\gamma\gamma j_F}$
Average number of interactions per bunch crossing.

Binary BDT: Training variables

Submitted to JHEP

STXS classes	Variables
Individual STXS classes from $gg \to H$, $qq' \to Hqq'$, $qq \to H\ell\nu$, $pp \to H\ell\ell$, $pp \to H\nu\bar{\nu}$	All multiclass BDT variables, $\boldsymbol{p}_{\mathrm{T}}^{\gamma\gamma}$ projected to the thrust axis of the $\gamma\gamma$ system ($p_{\mathrm{Tt}}^{\gamma\gamma}$), $\Delta\eta_{\gamma\gamma}$, $\eta^{\mathrm{Zepp}} = \frac{\eta_{\gamma\gamma}-\eta_{jj}}{2}$, $\phi^{*}_{\gamma\gamma} = \tan\left(\frac{\pi-\lvert\Delta\phi_{\gamma\gamma}\rvert}{2}\right)\sqrt{1-\tanh^{2}\left(\frac{\Delta\eta_{\gamma\gamma}}{2}\right)}$, $\cos\theta^{*}_{\gamma\gamma} = \left\lvert\frac{(E^{\gamma_1}+p_z^{\gamma_1})\cdot(E^{\gamma_2}-p_z^{\gamma_2})-(E^{\gamma_1}-p_z^{\gamma_1})\cdot(E^{\gamma_2}+p_z^{\gamma_2})}{m_{\gamma\gamma}+\sqrt{m_{\gamma\gamma}^{2}+(p_{\mathrm{T}}^{\gamma\gamma})^{2}}}\right\rvert$ Number of electrons and muons.
all $t\bar{t}H$ and tHW STXS classes combined	p_{T}, η, ϕ of γ_1 and γ_2, p_{T}, η, ϕ and b-tagging scores of the six highest-p_{T} jets, $E_{\mathrm{T}}^{\mathrm{miss}}$, $E_{\mathrm{T}}^{\mathrm{miss}}$ significance, $E_{\mathrm{T}}^{\mathrm{miss}}$ azimuthal angle, Top reconstruction BDT scores of the top-quark candidates, p_{T}, η, ϕ of the two highest-p_{T} leptons.
$tHqb$	$p_{\mathrm{T}}^{\gamma\gamma}/m_{\gamma\gamma}$, $\eta_{\gamma\gamma}$, p_{T}, invariant mass, BDT score and $\Delta R(W,b)$ of t_1, p_{T}, η of t_2, p_{T}, η of j_F, Angular variables: $\Delta\eta_{\gamma\gamma t_1}$, $\Delta\theta_{\gamma\gamma t_2}$, $\Delta\theta_{t_1 j_F}$, $\Delta\theta_{t_2 j_F}$, $\Delta\theta_{\gamma\gamma j_F}$ Invariant mass variables: $m_{\gamma\gamma j_F}$, $m_{t_1 j_F}$, $m_{t_2 j_F}$, $m_{\gamma\gamma t_1}$ Number of jets with $p_{\mathrm{T}} > 25$ GeV, Number of b-jets with $p_{\mathrm{T}} > 25$ GeV*; Number of leptons*, $E_{\mathrm{T}}^{\mathrm{miss}}$ significance*

Main improvement for HZZ

- Improved lepton isolation to mitigate the impact of pile-up
- Improved jet reconstruction using a particle flow algorithm
- Additional event categories for the classification of Higgs boson candidates
- New discriminants to enhance the sensitivity to distinguish the various production modes of the SM Higgs boson
- Use of data sidebands to constrain the dominant $ZZ*$ background process

H→WW*: analysis

Category	$N_{\text{jet},(p_T>30\text{ GeV})} = 0$ ggF	$N_{\text{jet},(p_T>30\text{ GeV})} = 1$ ggF	$N_{\text{jet},(p_T>30\text{ GeV})} \geq 2$ ggF	$N_{\text{jet},(p_T>30\text{ GeV})} \geq 2$ VBF
Preselection	Two isolated, different-flavor leptons ($\ell = e, \mu$) with opposite charge $p_T^{\text{lead}} > 22$ GeV , $p_T^{\text{sublead}} > 15$ GeV $m_{\ell\ell} > 10$ GeV			
	$p_T^{\text{miss}} > 20$ GeV			
Background rejection	$N_{b\text{-jet},(p_T>20\text{ GeV})} = 0$			
	$\Delta\phi_{\ell\ell,E_T^{\text{miss}}} > \pi/2$ $p_T^{\ell\ell} > 30$ GeV	$m_{\tau\tau} < m_Z - 25$ GeV		
		max $(m_T^{\ell}) > 50$ GeV		
$H \to WW^* \to e\nu\mu\nu$ topology	$m_{\ell\ell} < 55$ GeV $\Delta\phi_{\ell\ell} < 1.8$			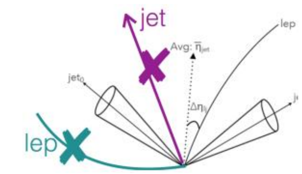 central jet veto outside lepton veto $m_{jj} > 120$ GeV
			fail central jet veto or fail outside lepton veto	
			$\lvert m_{jj} - 85\rvert > 15$ GeV or $\Delta y_{jj} > 1.2$	
Discriminating fit variable	m_T			DNN

Reconstructed with the collinear approximation method

Submitted to PRD

H→WW*: analysis

<table>
<tr><th>CR</th><th>$N_{\text{jet},(p_T>30\text{ GeV})}=0$ ggF</th><th>$N_{\text{jet},(p_T>30\text{ GeV})}=1$ ggF</th><th>$N_{\text{jet},(p_T>30\text{ GeV})}\geq 2$ ggF</th><th>$N_{\text{jet},(p_T>30\text{ GeV})}\geq 2$ VBF</th></tr>
<tr><td rowspan="5">$qq\to WW$</td><td colspan="3">$N_{b\text{-jet},(p_T>20\text{ GeV})}=0$</td><td rowspan="5"></td></tr>
<tr><td rowspan="4">$\Delta\phi_{\ell\ell,E_T^{\text{miss}}}>\pi/2$
$p_T^{\ell\ell}>30$ GeV
$55<m_{\ell\ell}<110$ GeV
$\Delta\phi_{\ell\ell}<2.6$</td><td colspan="2">$m_{\ell\ell}>80$ GeV</td></tr>
<tr><td rowspan="3">$|m_{\tau\tau}-m_Z|>25$ GeV
$\max\left(m_T^{\ell}\right)>50$ GeV</td><td>$m_{\tau\tau}<m_Z-25$ GeV
$m_{T2}>165$ GeV</td></tr>
<tr><td>fail central jet veto
or fail outside lepton veto</td></tr>
<tr><td>$|m_{jj}-85|>15$ GeV
or $\Delta y_{jj}>1.2$</td></tr>
<tr><td rowspan="5">$t\bar{t}/Wt$</td><td rowspan="5">$N_{b\text{-jet},(20<p_T<30\text{ GeV})}>0$

$\Delta\phi_{\ell\ell,E_T^{\text{miss}}}>\pi/2$
$p_T^{\ell\ell}>30$ GeV
$\Delta\phi_{\ell\ell}<2.8$</td><td>$N_{b\text{-jet},(p_T>30\text{ GeV})}=1$
$N_{b\text{-jet},(20<p_T<30\text{ GeV})}=0$</td><td>$N_{b\text{-jet},(p_T>20\text{ GeV})}=0$</td><td>$N_{b\text{-jet},(p_T>20\text{ GeV})}=1$</td></tr>
<tr><td colspan="3">$m_{\tau\tau}<m_Z-25$ GeV</td></tr>
<tr><td rowspan="3">$\max\left(m_T^{\ell}\right)>50$ GeV</td><td>$m_{\ell\ell}>80$ GeV
$\Delta\phi_{\ell\ell}<1.8$
$m_{T2}<165$ GeV</td><td rowspan="3">central jet veto
outside lepton veto</td></tr>
<tr><td>fail central jet veto
or fail outside lepton veto</td></tr>
<tr><td>$|m_{jj}-85|>15$ GeV
or $\Delta y_{jj}>1.2$</td></tr>
<tr><td rowspan="5">Z/γ^*</td><td colspan="4">$N_{b\text{-jet},(p_T>20\text{ GeV})}=0$</td></tr>
<tr><td colspan="2">$m_{\ell\ell}<80$ GeV
no p_T^{miss} requirement</td><td>$m_{\ell\ell}<55$ GeV</td><td rowspan="4">$m_{\ell\ell}<70$ GeV

$|m_{\tau\tau}-m_Z|\leq 25$ GeV
central jet veto
outside lepton veto</td></tr>
<tr><td rowspan="3">$\Delta\phi_{\ell\ell}>2.8$</td><td colspan="2">$m_{\tau\tau}>m_Z-25$ GeV</td></tr>
<tr><td rowspan="2">$\max\left(m_T^{\ell}\right)>50$ GeV</td><td>fail central jet veto
or fail outside lepton veto</td></tr>
<tr><td>$|m_{jj}-85|>15$ GeV
or $\Delta y_{jj}>1.2$</td></tr>
</table>

Submitted to PRD

VBF ≥2 Jet: Deep Neural Network (DNN)

Submitted to PRD

DNN inputs:

$$\Delta\phi_{\ell\ell}, m_{\ell\ell}, m_{\mathrm{T}}, \Delta y_{jj}, m_{jj}, p_{\mathrm{T}}^{\mathrm{tot}}, \eta_{\ell}^{\mathrm{centrality}}, m_{\ell1j1}, m_{\ell1j2}, m_{\ell2j1}, m_{\ell2j2},$$
$$p_{\mathrm{T}}^{\mathrm{jet}_1}, p_{\mathrm{T}}^{\mathrm{jet}_2}, p_{\mathrm{T}}^{\mathrm{jet}_3}, \text{ and MET significance}$$

Training done after preselection, b veto && $m_{\tau\tau} < m_Z - 25\ \mathrm{GeV}$

Training target: VBF VS all bkg(ggF, ttbar, ww*..)

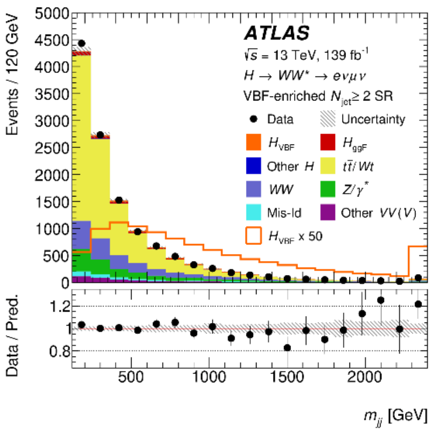

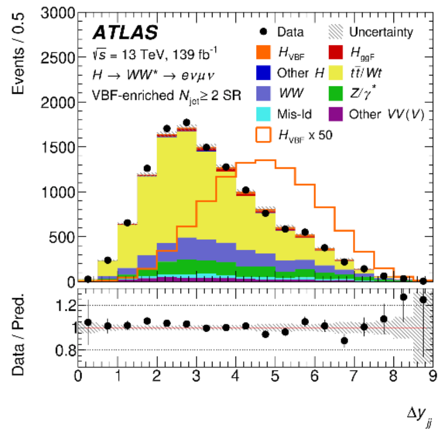

Two most powerful variables

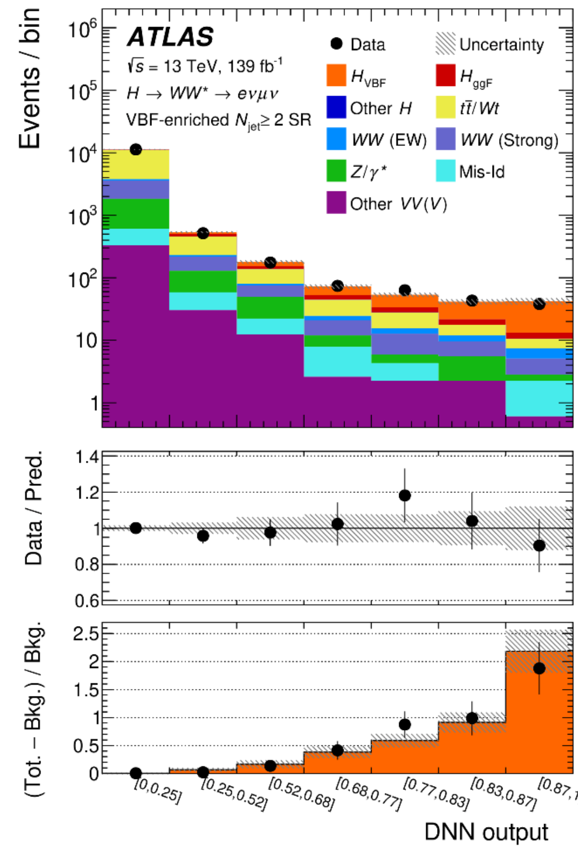

H→WW*: analysis

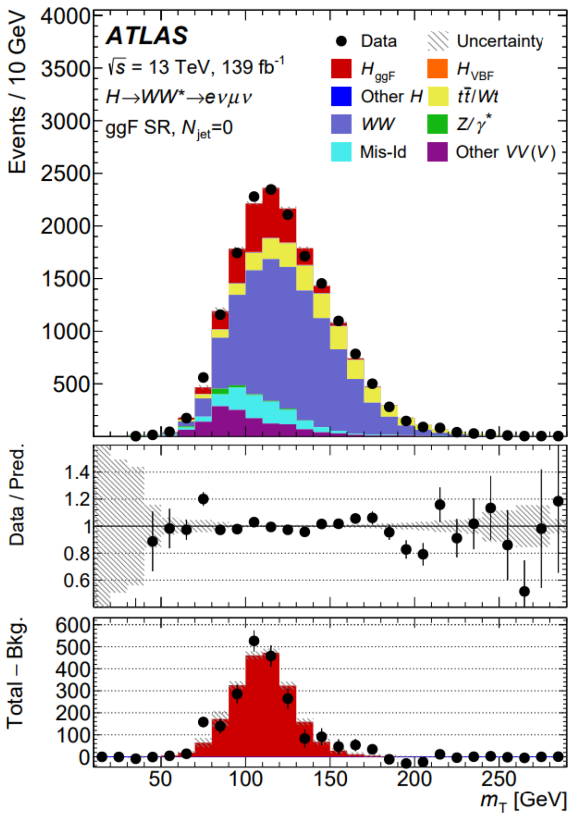

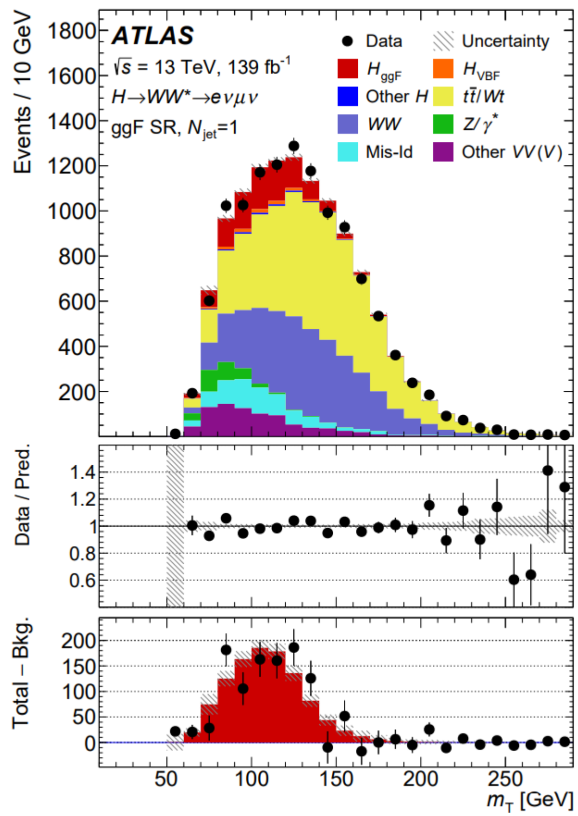

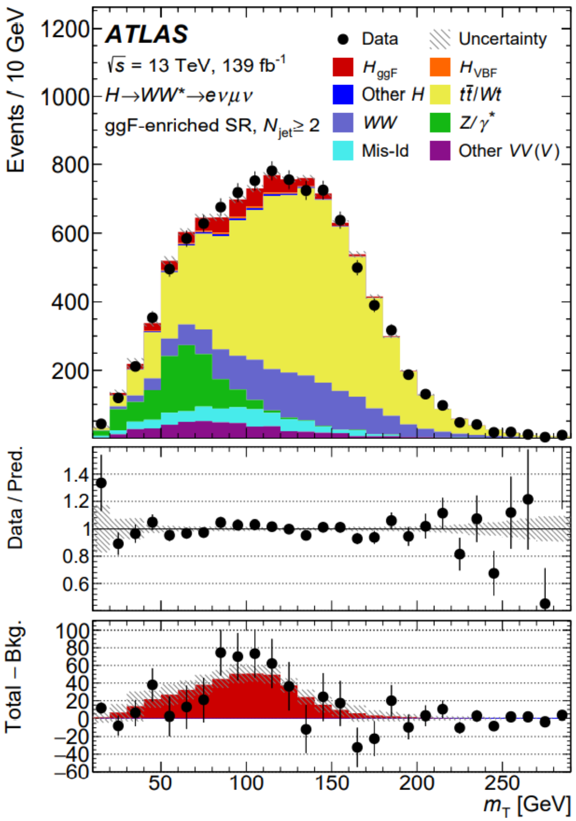

[Submitted to PRD]()

$H \to WW^*$: Break down

Source	$\frac{\Delta\sigma_{ggF+VBF}\cdot\mathcal{B}_{H\to WW^*}}{\sigma_{ggF+VBF}\cdot\mathcal{B}_{H\to WW^*}}$ [%]	$\frac{\Delta\sigma_{ggF}\cdot\mathcal{B}_{H\to WW^*}}{\sigma_{ggF}\cdot\mathcal{B}_{H\to WW^*}}$ [%]	$\frac{\Delta\sigma_{VBF}\cdot\mathcal{B}_{H\to WW^*}}{\sigma_{VBF}\cdot\mathcal{B}_{H\to WW^*}}$ [%]
Data statistical uncertainties	4.6	5.1	15
Total systematic uncertainties	9.5	11	18
MC statistical uncertainties	3.0	3.8	4.9
Experimental uncertainties	5.2	6.3	6.7
Flavor tagging	2.3	2.7	1.0
Jet energy scale	0.9	1.1	3.7
Jet energy resolution	2.0	2.4	2.1
E_T^{miss}	0.7	2.2	4.9
Muons	1.8	2.1	0.8
Electrons	1.3	1.6	0.4
Fake factors	2.1	2.4	0.8
Pileup	2.4	2.5	1.3
Luminosity	2.1	2.0	2.2
Theoretical uncertainties	6.8	7.8	16
ggF	3.8	4.3	4.6
VBF	3.2	0.7	12
WW	3.5	4.2	5.5
Top	2.9	3.8	6.4
$Z\tau\tau$	1.8	2.3	1.0
Other VV	2.3	2.9	1.5
Other Higgs	0.9	0.4	0.4
Background normalizations	3.6	4.5	4.9
WW	2.2	2.8	0.6
Top	1.9	2.3	3.4
$Z\tau\tau$	2.7	3.1	3.4
Total	10	12	23

H→WW*: STXS

Submitted to PRD

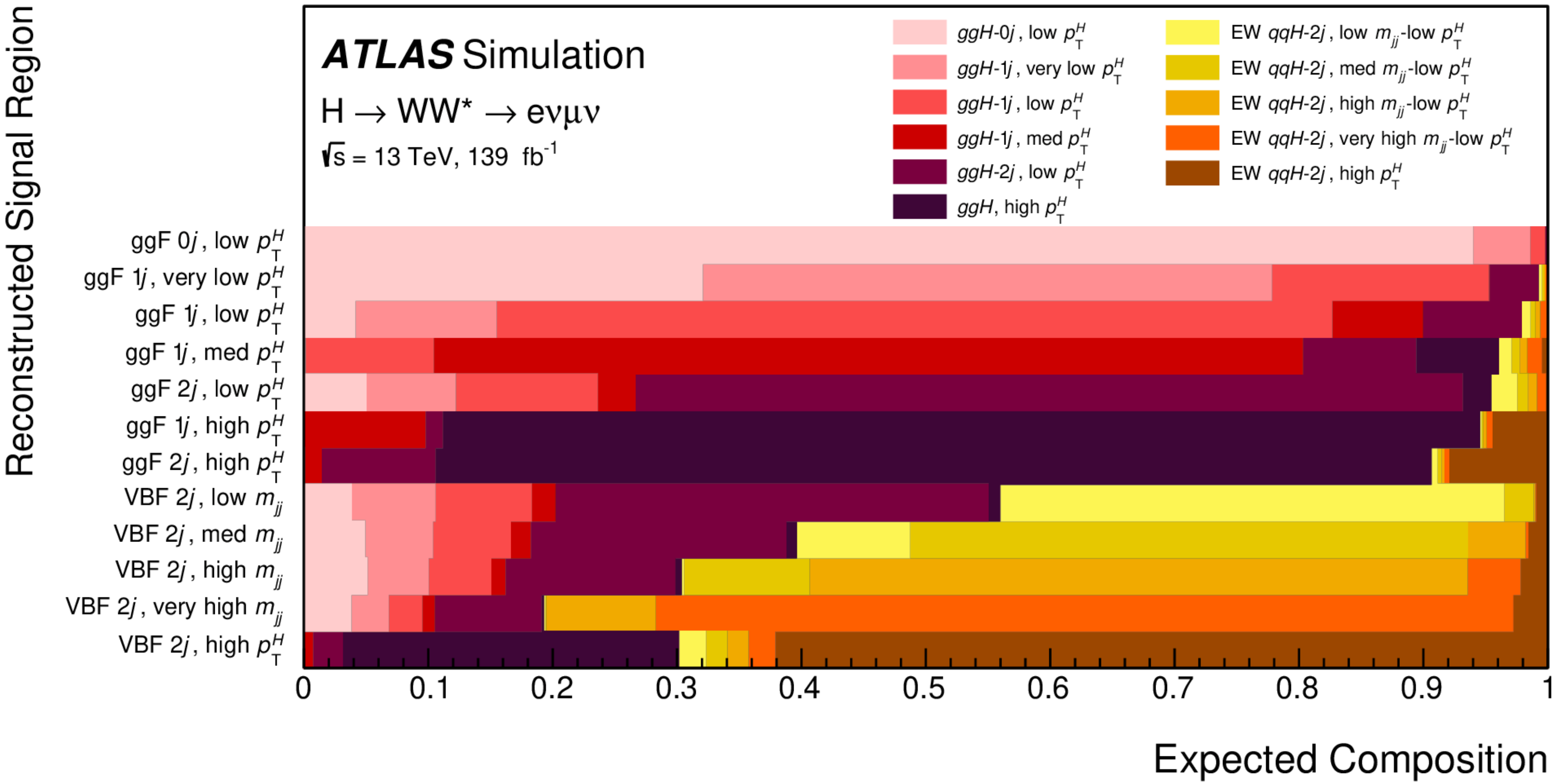

H→WW*: STXS

Submitted to PRD

Statistically dominant for most categories

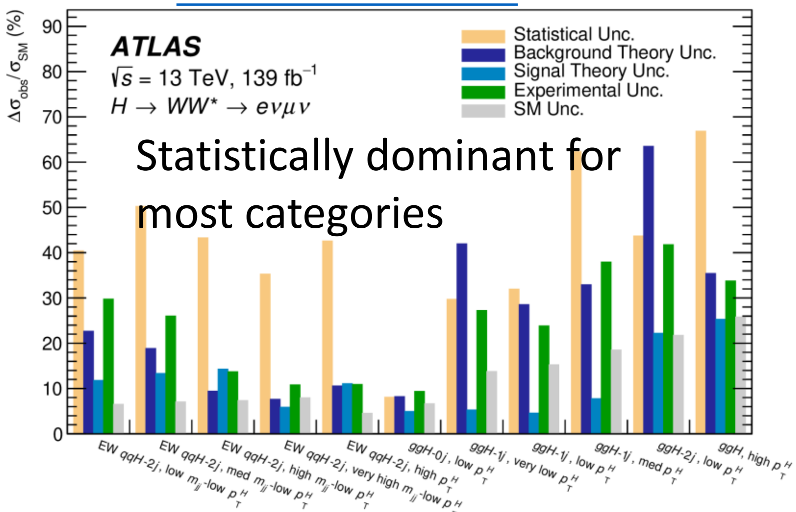

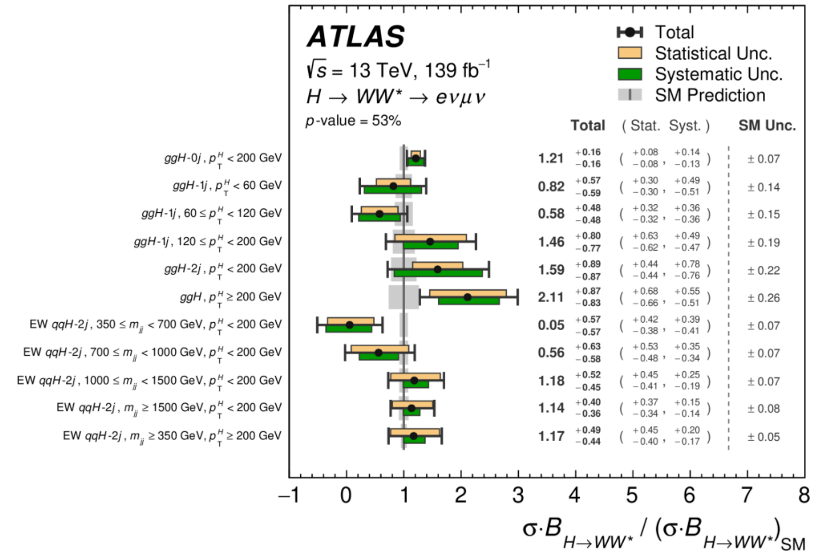

STXS bin ($\sigma_i \cdot \mathcal{B}_{H\to WW^*}$)	Value [fb]	Uncertainty [fb] Total	Stat.	Exp. Syst.	Sig. Theo.	Bkg. Theo.	SM prediction [fb]
ggH-0j, low p_T^H, p_T^H < 200 GeV	7100	$^{+950}_{-910}$	$^{+480}_{-470}$	$^{+570}_{-530}$	$^{+320}_{-260}$	$^{+490}_{-480}$	5870 ± 390
ggH-1j, very low p_T^H, p_T^H < 60 GeV	1140	$^{+800}_{-820}$	$^{+420}_{-410}$	$^{+380}_{-380}$	$^{+80}_{-70}$	$^{+570}_{-600}$	1400 ± 190
ggH-1j, low p_T^H, 60 ≤ p_T^H < 120 GeV	540	$^{+470}_{-470}$	$^{+310}_{-310}$	$^{+230}_{-230}$	$^{+42}_{-47}$	$^{+270}_{-280}$	970 ± 150
ggH-1j, med p_T^H, 120 ≤ p_T^H < 200 GeV	230	$^{+130}_{-120}$	$^{+100}_{-100}$	$^{+60}_{-60}$	$^{+10}_{-10}$	$^{+50}_{-50}$	160 ± 30
ggH-2j, low p_T^H, p_T^H < 200 GeV	1610	$^{+900}_{-890}$	$^{+440}_{-440}$	$^{+430}_{-420}$	$^{+300}_{-150}$	$^{+640}_{-650}$	1010 ± 220
ggH, high p_T^H, p_T^H ≥ 200 GeV	260	$^{+100}_{-100}$	$^{+80}_{-80}$	$^{+40}_{-40}$	$^{+40}_{-20}$	$^{+40}_{-40}$	122 ± 31
EW qqH-2j, low m_{jj}-low p_T^H, 350 ≤ m_{jj} < 700 GeV, p_T^H < 200 GeV	6	$^{+63}_{-62}$	$^{+46}_{-42}$	$^{+31}_{-34}$	$^{+11}_{-14}$	$^{+24}_{-26}$	109 ± 7
EW qqH-2j, med m_{jj}-low p_T^H, 700 ≤ m_{jj} < 1000 GeV, p_T^H < 200 GeV	31	$^{+35}_{-33}$	$^{+30}_{-27}$	$^{+15}_{-14}$	$^{+8}_{-7}$	$^{+11}_{-10}$	56 ± 4
EW qqH-2j, high m_{jj}-low p_T^H, 1000 ≤ m_{jj} < 1500 GeV, p_T^H < 200 GeV	60	$^{+26}_{-23}$	$^{+23}_{-21}$	$^{+7}_{-7}$	$^{+9}_{-5}$	$^{+5}_{-5}$	51 ± 4
EW qqH-2j, very high m_{jj}-low p_T^H, m_{jj} ≥ 1500 GeV, p_T^H < 200 GeV	57	$^{+20}_{-18}$	$^{+18}_{-17}$	$^{+5}_{-5}$	$^{+3}_{-3}$	$^{+4}_{-4}$	50 ± 4
EW qqH-2j, high p_T^H, m_{jj} ≥ 350 GeV, p_T^H ≥ 200 GeV	37	$^{+16}_{-14}$	$^{+14}_{-13}$	$^{+4}_{-3}$	$^{+4}_{-3}$	$^{+3}_{-3}$	32 ± 1

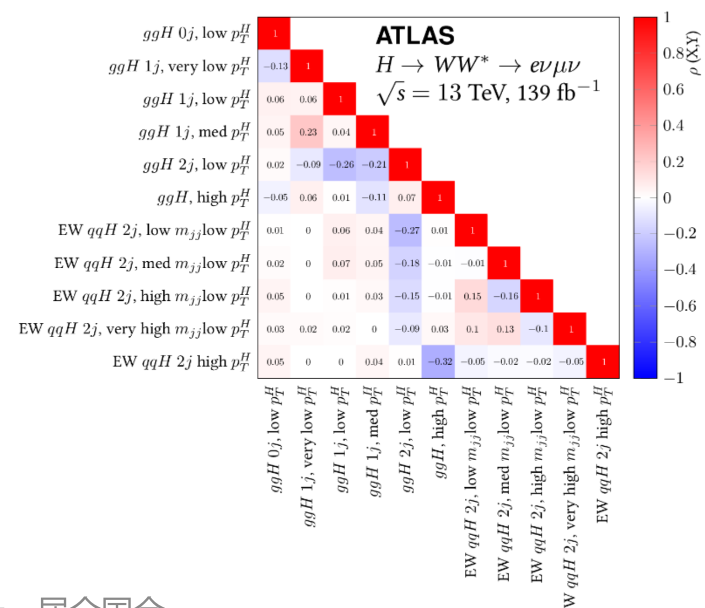

H→ZZ*: STXS

Eur. Phys. J. C 80, 957 (2020).

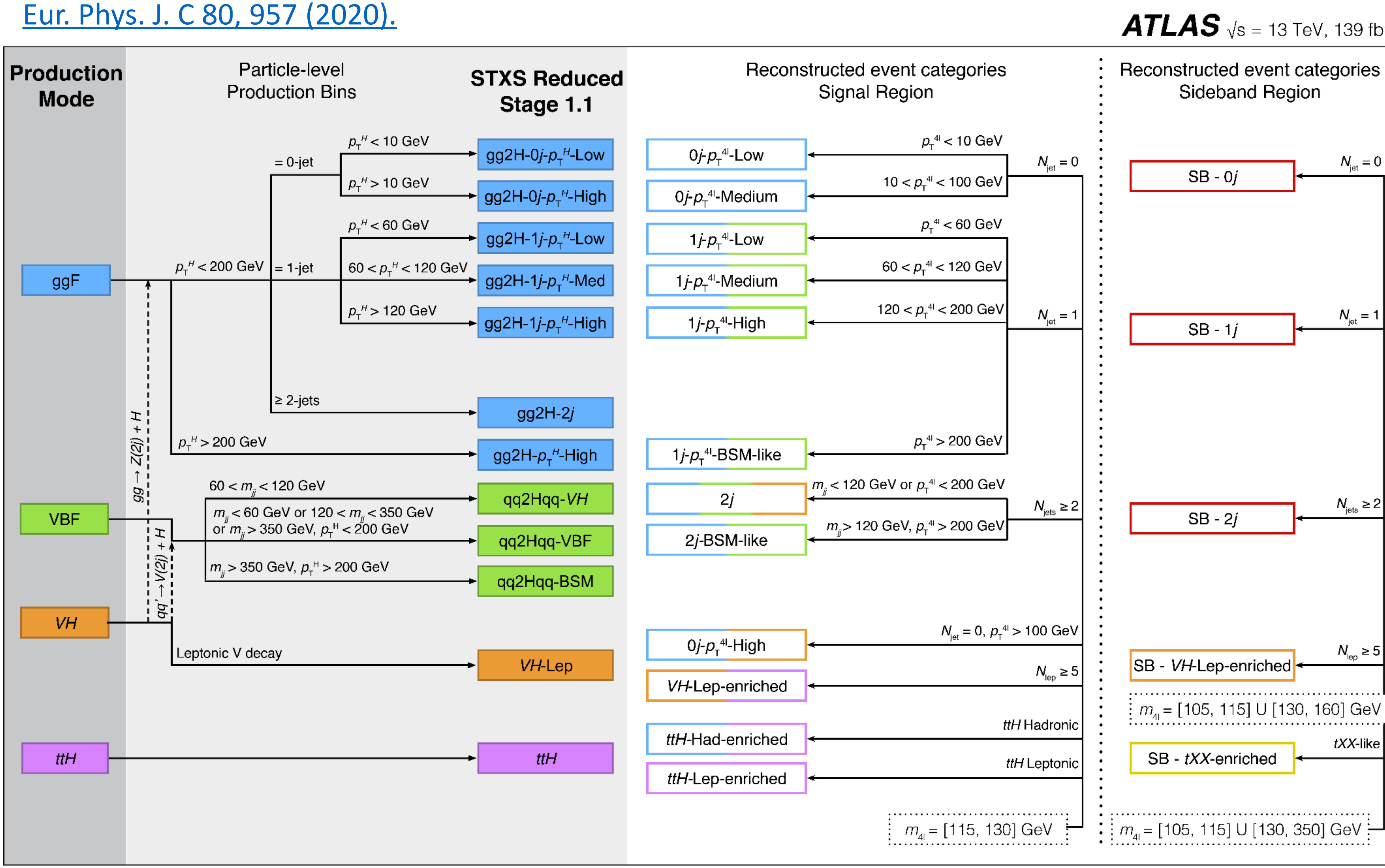

H→ZZ*: STXS

Eur. Phys. J. C 80, 957 (2020).

- Two types of NNs are used: feed-forward multilayer perceptron (MLP) and recurrent (RNN)
- The input variables used to train the MLP, and the two RNNs for the four leptons and the jets

Category	Processes	MLP	Lepton RNN	Jet RNN	Discriminant
$0j$-$p_T^{4\ell}$-Low $0j$-$p_T^{4\ell}$-Med	ggF, ZZ^*	$p_T^{4\ell}$, D_{ZZ^*}, m_{12}, m_{34}, $\lvert\cos\theta^*\rvert$, $\cos\theta_1$, ϕ_{ZZ}	p_T^ℓ, η_ℓ	-	$\mathrm{NN}_{\mathrm{ggF}}$
$1j$-$p_T^{4\ell}$-Low	ggF, VBF, ZZ^*	$p_T^{4\ell}$, p_T^j, η_j, $\Delta R_{4\ell j}$, D_{ZZ^*}	p_T^ℓ, η_ℓ	-	$\mathrm{NN}_{\mathrm{VBF}}$ for $\mathrm{NN}_{ZZ} < 0.25$ NN_{ZZ} for $\mathrm{NN}_{ZZ} > 0.25$
$1j$-$p_T^{4\ell}$-Med	ggF, VBF, ZZ^*	$p_T^{4\ell}$, p_T^j, η_j, E_T^{miss}, $\Delta R_{4\ell j}$, D_{ZZ^*}, $\eta_{4\ell}$	p_T^ℓ, η_ℓ	-	$\mathrm{NN}_{\mathrm{VBF}}$ for $\mathrm{NN}_{ZZ} < 0.25$ NN_{ZZ} for $\mathrm{NN}_{ZZ} > 0.25$
$1j$-$p_T^{4\ell}$-High	ggF, VBF	$p_T^{4\ell}$, p_T^j, η_j, E_T^{miss}, $\Delta R_{4\ell j}$, $\eta_{4\ell}$	p_T^ℓ, η_ℓ	-	$\mathrm{NN}_{\mathrm{VBF}}$
$2j$	ggF, VBF, VH	m_{jj}, $p_T^{4\ell jj}$	p_T^ℓ, η_ℓ	p_T^j, η_j	$\mathrm{NN}_{\mathrm{VBF}}$ for $\mathrm{NN}_{VH} < 0.2$ NN_{VH} for $\mathrm{NN}_{VH} > 0.2$
$2j$-BSM-like	ggF, VBF	$\eta_{ZZ}^{\mathrm{Zepp}}$, $p_T^{4\ell jj}$	p_T^ℓ, η_ℓ	p_T^j, η_j	$\mathrm{NN}_{\mathrm{VBF}}$
VH-Lep-enriched	VH, ttH	N_{jets}, $N_{b\text{-jets},70\%}$, E_T^{miss}, H_T	p_T^ℓ	-	NN_{ttH}
ttH-Had-enriched	ggF, ttH, tXX	$p_T^{4\ell}$, m_{jj}, $\Delta R_{4\ell j}$, $N_{b\text{-jets},70\%}$,	p_T^ℓ, η_ℓ	p_T^j, η_j	NN_{ttH} for $\mathrm{NN}_{tXX} < 0.4$ NN_{tXX} for $\mathrm{NN}_{tXX} > 0.4$

H→ZZ*: STXS

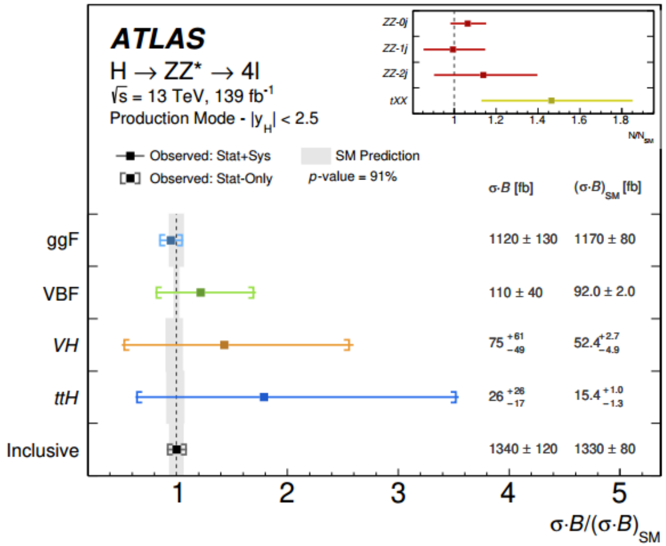

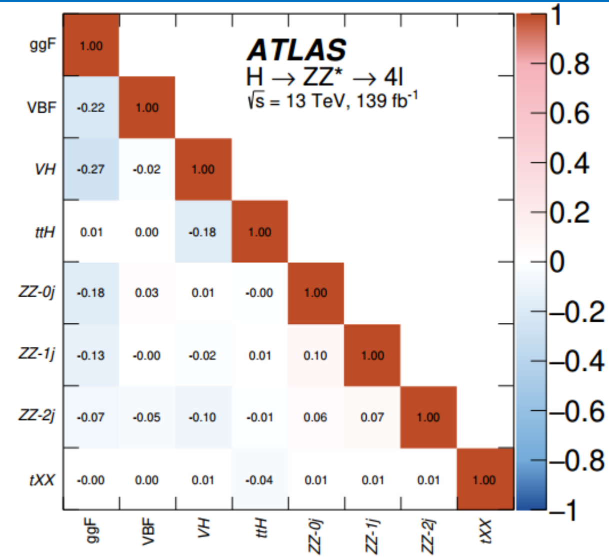

Eur. Phys. J. C 80, 957 (2020).

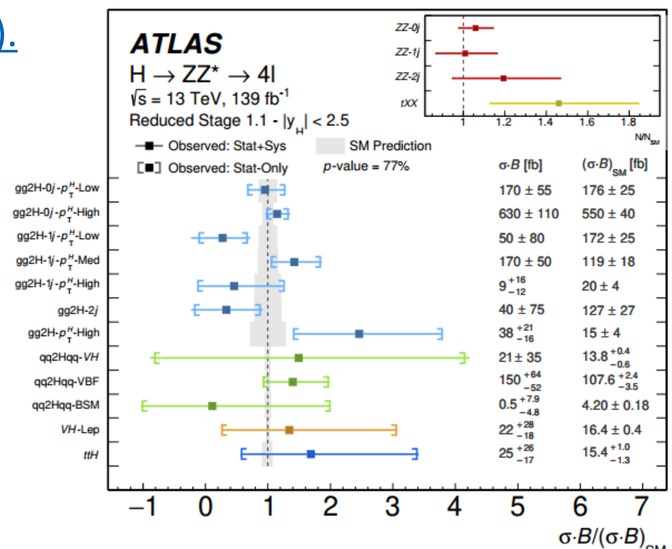

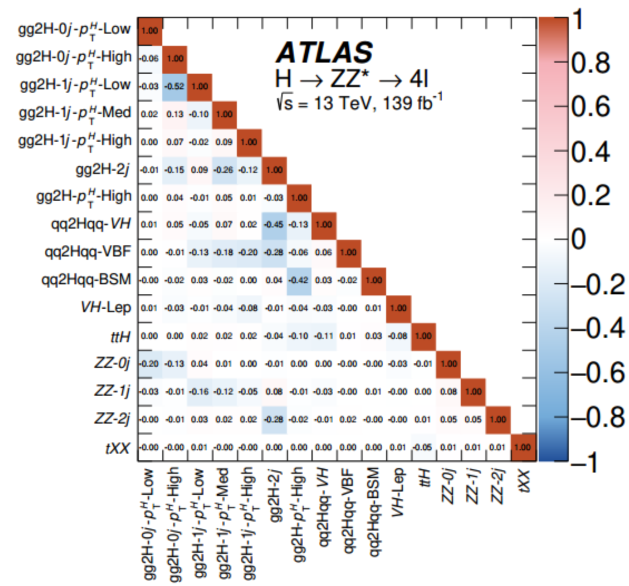

H→ZZ*: STXS

Measurement	Experimental uncertainties [%] Lumi.	e, μ, pile-up	Jets, flav. tag	Reducible bkg	Theory uncertainties [%] Background ZZ^*	tXX	Signal PDF	QCD	Shower
Inclusive cross-section									
	1.7	2.5	0.5	< 0.5	1	< 0.5	< 0.5	1	2
Production mode cross-sections									
ggF	1.7	2.5	1	< 0.5	1.5	< 0.5	0.5	1	2
VBF	1.7	2	4	< 0.5	1.5	< 0.5	1	5	7
VH	1.9	2	4	1	6	< 0.5	2	13.5	7.5
ttH	1.7	2	6	< 0.5	1	0.5	0.5	12.5	4
Reduced Stage-1.1 production bin cross-sections									
gg2H-0j-p_T^H-Low	1.7	3	1.5	0.5	6.5	< 0.5	< 0.5	1	1.5
gg2H-0j-p_T^H-High	1.7	3	5	< 0.5	3	< 0.5	< 0.5	0.5	5.5
gg2H-1j-p_T^H-Low	1.7	2.5	12	0.5	7	< 0.5	< 0.5	1	6
gg2H-1j-p_T^H-Med	1.7	3	7.5	< 0.5	1	< 0.5	< 0.5	1.5	5.5
gg2H-1j-p_T^H-High	1.7	3	11	0.5	2	< 0.5	< 0.5	2	7.5
gg2H-2j	1.7	2.5	16.5	1	12.5	0.5	< 0.5	2.5	10.5
gg2H-p_T^H-High	1.7	1.5	3	0.5	3.5	< 0.5	< 0.5	2	3.5
qq2Hqq-VH	1.8	4	17	1	4	1	0.5	5.5	8
qq2Hqq-VBF	1.7	2	3.5	< 0.5	5	< 0.5	< 0.5	6	10.5
qq2Hqq-BSM	1.7	2	4	< 0.5	2.5	< 0.5	< 0.5	3	8
VH-Lep	1.8	2.5	2	1	2	0.5	< 0.5	1.5	3
ttH	1.7	2.5	5	0.5	1	0.5	< 0.5	11	3

Eur. Phys. J. C 80, 957 (2020).

- The luminosity uncertainty, which is measured to be 1.7% and increases for the VH signal processes due to the simulation-based normalisation of the background.

$H \rightarrow \gamma\gamma$: 45 STXS analysis region

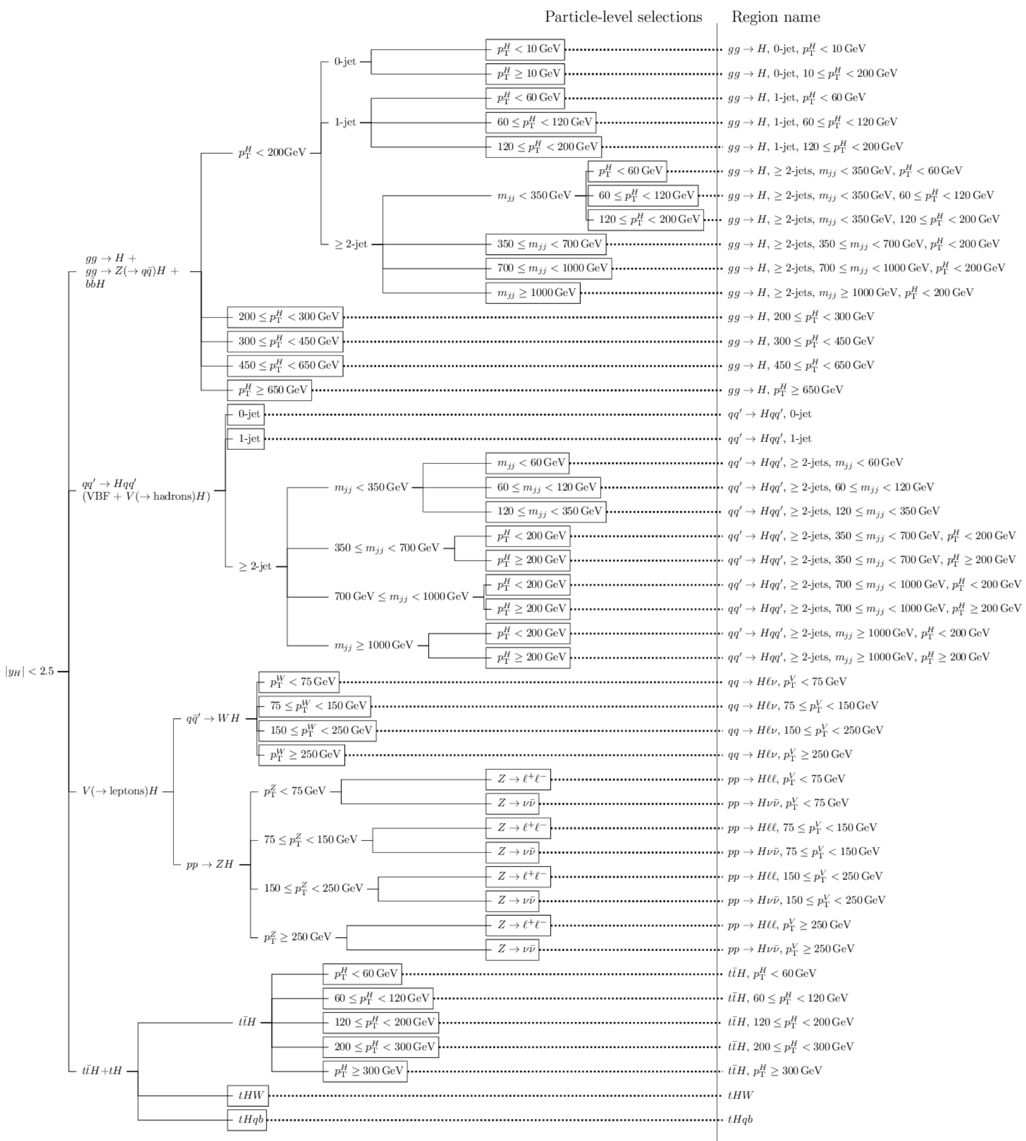

[Submitted to JHEP]

$H \rightarrow \gamma\gamma$:101 analysis categories

Category	Function	N_{data}	N_{spur}	Wald
$gg \rightarrow H$				
0-jet, $p_T^H < 10$ GeV	ExpPoly2	191623	64.8	
0-jet, $p_T^H \geq 10$ GeV	ExpPoly2	349266	50.4	
1-jet, $p_T^H < 60$ GeV, High-purity	ExpPoly2	32644	20.7	
1-jet, $p_T^H < 60$ GeV, Med-purity	ExpPoly2	85229	24.9	
1-jet, $60 \leq p_T^H < 120$ GeV, High-purity	Exp	26236	23.7	
1-jet, $60 \leq p_T^H < 120$ GeV, Med-purity	ExpPoly2	56669	21.3	
1-jet, $120 \leq p_T^H < 200$ GeV, High-purity	ExpPoly2	1570	1.48	
1-jet, $120 \leq p_T^H < 200$ GeV, Med-purity	ExpPoly2	6163	5.33	
$\geq$ 2-jets, $m_{jj} < 350$ GeV, $p_T^H < 60$ GeV, High-purity	ExpPoly2	8513	1.51	
$\geq$ 2-jets, $m_{jj} < 350$ GeV, $p_T^H < 60$ GeV, Med-purity	ExpPoly2	31163	13.6	
$\geq$ 2-jets, $m_{jj} < 350$ GeV, $p_T^H < 60$ GeV, Low-purity	ExpPoly2	120357	15.7	
$\geq$ 2-jets, $m_{jj} < 350$ GeV, $60 \leq p_T^H < 120$ GeV, High-purity	ExpPoly2	7582	2.26	
$\geq$ 2-jets, $m_{jj} < 350$ GeV, $60 \leq p_T^H < 120$ GeV, Med-purity	ExpPoly2	48362	6.21	
$\geq$ 2-jets, $m_{jj} < 350$ GeV, $120 \leq p_T^H < 200$ GeV, High-purity	ExpPoly2	728	0.004	
$\geq$ 2-jets, $m_{jj} < 350$ GeV, $120 \leq p_T^H < 200$ GeV, Med-purity	PowerLaw	3007	0.983	
$\geq$ 2-jets, $350 \leq m_{jj} < 700$ GeV, $p_T^H < 200$ GeV, High-purity	Exp	432	0.487	
$\geq$ 2-jets, $350 \leq m_{jj} < 700$ GeV, $p_T^H < 200$ GeV, Med-purity	ExpPoly2	3084	1.33	
$\geq$ 2-jets, $350 \leq m_{jj} < 700$ GeV, $p_T^H < 200$ GeV, Low-purity	Exp	7999	5.78	
$\geq$ 2-jets, $700 \leq m_{jj} < 1000$ GeV, $p_T^H < 200$ GeV, High-purity	Exp	302	0.560	
$\geq$ 2-jets, $700 \leq m_{jj} < 1000$ GeV, $p_T^H < 200$ GeV, Med-purity	Exp	1033	1.44	
$\geq$ 2-jets, $700 \leq m_{jj} < 1000$ GeV, $p_T^H < 200$ GeV, Low-purity	Exp	3187	4.32	
$\geq$ 2-jets, $m_{jj} \geq 1000$ GeV, $p_T^H < 200$ GeV, High-purity	Exp	113	0.192	
$\geq$ 2-jets, $m_{jj} \geq 1000$ GeV, $p_T^H < 200$ GeV, Med-purity	Exp	332	0.804	
$\geq$ 2-jets, $m_{jj} \geq 1000$ GeV, $p_T^H < 200$ GeV, Low-purity	PowerLaw	1020	1.09	
$200 \leq p_T^H < 300$ GeV, High-purity	Exp	420	1.68	
$200 \leq p_T^H < 300$ GeV, Med-purity	Exp	2296	0.714	
$300 \leq p_T^H < 450$ GeV, High-purity	Exp	25	0.407	✓
$300 \leq p_T^H < 450$ GeV, Med-purity	Exp	186	0.259	
$300 \leq p_T^H < 450$ GeV, Low-purity	Exp	422	0.121	
$450 \leq p_T^H < 650$ GeV, High-purity	Exp	15	0.138	✓
$450 \leq p_T^H < 650$ GeV, Med-purity	Exp	25	0.391	✓
$450 \leq p_T^H < 650$ GeV, Low-purity	Exp	109	0.031	
$p_T^H \geq 650$ GeV	Exp	14	0.448	✓
$qq' \rightarrow Hqq'$				
0-jet, High-purity	Exp	176	0.180	
0-jet, Med-purity	ExpPoly2	3238	4.73	
0-jet, Low-purity	ExpPoly2	133314	49.7	
1-jet, High-purity	Exp	19	0.125	✓
1-jet, Med-purity	Exp	187	0.361	
1-jet, Low-purity	PowerLaw	1040	1.97	
$\geq$ 2-jets, $m_{jj} < 60$ GeV, High-purity	Exp	17	0.499	✓
$\geq$ 2-jets, $m_{jj} < 60$ GeV, Med-purity	Exp	157	0.489	
$\geq$ 2-jets, $m_{jj} < 60$ GeV, Low-purity	PowerLaw	1978	1.29	
$\geq$ 2-jets, $60 \leq m_{jj} < 120$ GeV, High-purity	Exp	53	0.165	✓
$\geq$ 2-jets, $60 \leq m_{jj} < 120$ GeV, Med-purity	Exp	329	0.520	
$\geq$ 2-jets, $60 \leq m_{jj} < 120$ GeV, Low-purity	PowerLaw	709	1.15	
$\geq$ 2-jets, $120 \leq m_{jj} < 350$ GeV, High-purity	Exp	214	1.08	
$\geq$ 2-jets, $120 \leq m_{jj} < 350$ GeV, Med-purity	ExpPoly2	1671	1.07	
$\geq$ 2-jets, $120 \leq m_{jj} < 350$ GeV, Low-purity	PowerLaw	11195	6.34	
$\geq$ 2-jets, $350 \leq m_{jj} < 700$ GeV, $p_T^H < 200$ GeV, High-purity	Exp	25	0.162	✓
$\geq$ 2-jets, $350 \leq m_{jj} < 700$ GeV, $p_T^H < 200$ GeV, Med-purity	Exp	260	0.443	
$\geq$ 2-jets, $350 \leq m_{jj} < 700$ GeV, $p_T^H < 200$ GeV, Low-purity	Exp	753	1.17	
$\geq$ 2-jets, $700 \leq m_{jj} < 1000$ GeV, $p_T^H < 200$ GeV, High-purity	Exp	25	0.670	✓
$\geq$ 2-jets, $700 \leq m_{jj} < 1000$ GeV, $p_T^H < 200$ GeV, Med-purity	Exp	166	0.713	
$\geq$ 2-jets, $m_{jj} \geq 1000$ GeV, $p_T^H < 200$ GeV, High-purity	Exp	48	1.47	✓
$\geq$ 2-jets, $m_{jj} \geq 1000$ GeV, $p_T^H < 200$ GeV, Med-purity	Exp	142	0.270	

Category	Function	N_{data}	N_{spur}	Wald
$\geq$ 2-jets, $350 \leq m_{jj} < 700$ GeV, $p_T^H \geq 200$ GeV, High-purity	Exp	18	0.189	✓
$\geq$ 2-jets, $350 \leq m_{jj} < 700$ GeV, $p_T^H \geq 200$ GeV, Med-purity	Exp	84	0.513	✓
$\geq$ 2-jets, $350 \leq m_{jj} < 700$ GeV, $p_T^H \geq 200$ GeV, Low-purity	Exp	595	0.721	
$\geq$ 2-jets, $700 \leq m_{jj} < 1000$ GeV, $p_T^H \geq 200$ GeV, High-purity	Exp	19	0.110	✓
$\geq$ 2-jets, $700 \leq m_{jj} < 1000$ GeV, $p_T^H \geq 200$ GeV, Med-purity	Exp	411	0.193	
$\geq$ 2-jets, $m_{jj} \geq 1000$ GeV, $p_T^H \geq 200$ GeV, High-purity	Exp	23	1.30	✓
$\geq$ 2-jets, $m_{jj} \geq 1000$ GeV, $p_T^H \geq 200$ GeV, Med-purity	Exp	56	0.329	✓
$qq \rightarrow H\ell\nu$				
$0 \leq p_T^V < 75$ GeV, High-purity	Exp	40	0.277	
$0 \leq p_T^V < 75$ GeV, Med-purity	Exp	158	0.609	
$75 \leq p_T^V < 150$ GeV, High-purity	Exp	15	0.069	
$75 \leq p_T^V < 150$ GeV, Med-purity	Exp	104	0.255	
$150 \leq p_T^V < 250$ GeV, High-purity	Exp	17	0.128	✓
$150 \leq p_T^V < 250$ GeV, Med-purity	Exp	21	0.150	
$p_T^V \geq 250$ GeV, High-purity	Exp	16	0.237	✓
$p_T^V \geq 250$ GeV, Med-purity	Exp	27	0.054	✓
$pp \rightarrow H\ell\ell$				
$0 \leq p_T^V < 75$ GeV, High-purity	Exp	12	0.027	
$0 \leq p_T^V < 75$ GeV, Med-purity	PowerLaw	1620	2.28	
$75 \leq p_T^V < 150$ GeV, High-purity	Exp	13	0.015	
$75 \leq p_T^V < 150$ GeV, Med-purity	Exp	18	0.016	
$150 \leq p_T^V < 250$ GeV, High-purity	Exp	14	0.059	✓
$150 \leq p_T^V < 250$ GeV, Med-purity	Exp	136	0.194	
$p_T^V \geq 250$ GeV	Exp	14	0.311	✓
$pp \rightarrow H\nu\bar{\nu}$				
$0 \leq p_T^V < 75$ GeV, High-purity	Exp	1174	12.3	✓
$0 \leq p_T^V < 75$ GeV, Med-purity	Exp	6897	4.13	
$0 \leq p_T^V < 75$ GeV, Low-purity	ExpPoly3	18084	9.95	
$75 \leq p_T^V < 150$ GeV, High-purity	Exp	16	0.407	✓
$75 \leq p_T^V < 150$ GeV, Med-purity	Exp	124	1.30	✓
$75 \leq p_T^V < 150$ GeV, Low-purity	Exp	2019	1.96	
$150 \leq p_T^V < 250$ GeV, High-purity	Exp	16	0.121	✓
$150 \leq p_T^V < 250$ GeV, Med-purity	Exp	17	0.184	✓
$150 \leq p_T^V < 250$ GeV, Low-purity	Exp	87	0.644	✓
$p_T^V \geq 250$ GeV, High-purity	Exp	15	0.237	✓
$p_T^V \geq 250$ GeV, Med-purity	Exp	18	0.201	✓
$t\bar{t}H$				
$p_T^H < 60$ GeV, High-purity	Exp	35	0.040	
$p_T^H < 60$ GeV, Med-purity	Exp	96	0.192	
$60 \leq p_T^H < 120$ GeV, High-purity	Exp	34	0.038	
$60 \leq p_T^H < 120$ GeV, Med-purity	Exp	74	0.274	
$120 \leq p_T^H < 200$ GeV, High-purity	Exp	39	0.018	
$120 \leq p_T^H < 200$ GeV, Med-purity	Exp	37	0.057	
$200 \leq p_T^H < 300$ GeV	Exp	23	0.261	
$p_T^H \geq 300$ GeV	Exp	19	0.180	✓
tH				
$tHqb$, High-purity	Exp	17	0.371	✓
$tHqb$, Med-purity	Exp	19	0.320	✓
$tHqb$, BSM ($\kappa_t = -1$)	Exp	14	0.496	✓
tHW	Exp	38	0.070	
Low-purity top	Exp	500	0.870	

Submitted to JHEP

$H \to \gamma\gamma$: Measured STXS (28 pois)

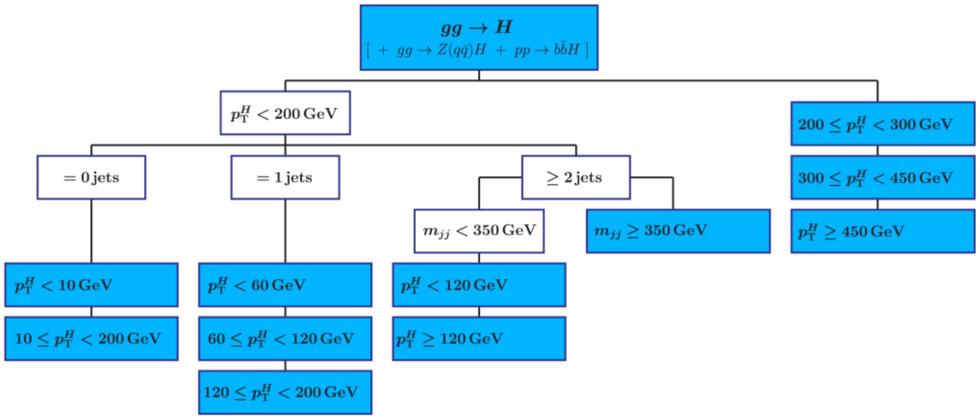

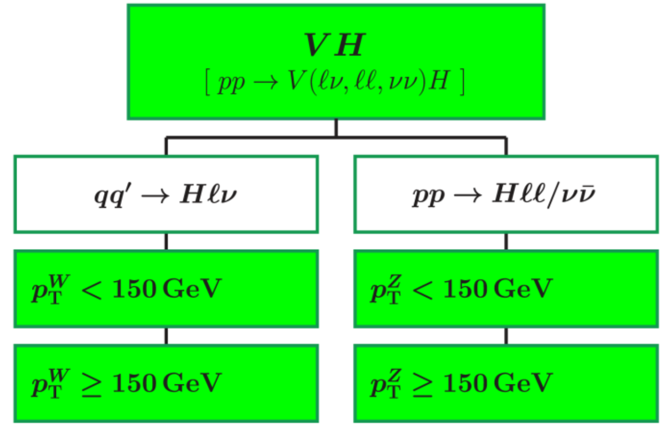

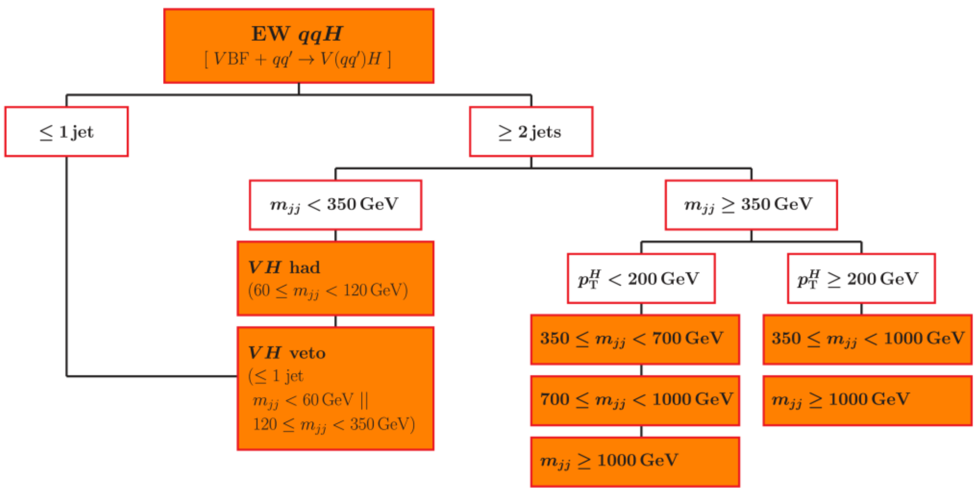

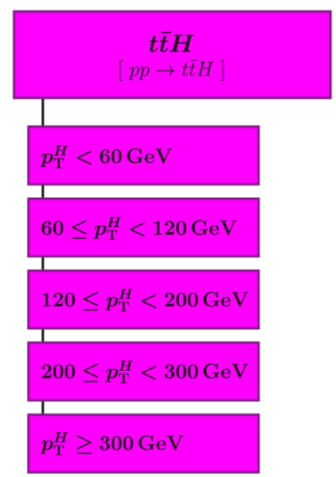

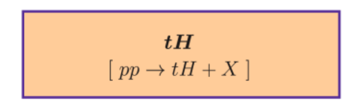

Submitted to JHEP

H⟶γγ: Production Mode Cross Sections

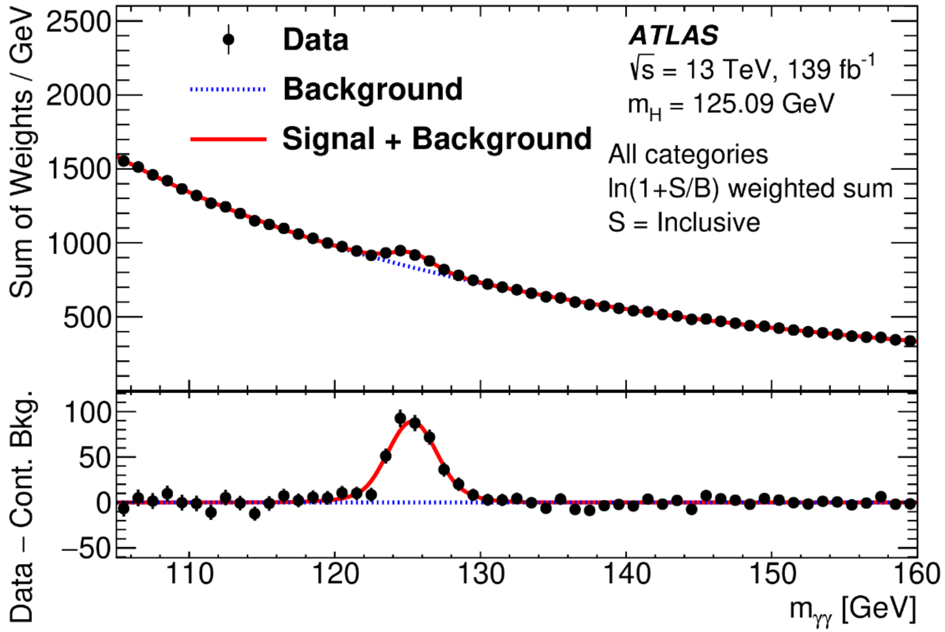

[Submitted to JHEP]

The events in each category are weighted by ln(1+S/B)

The fitted signal-plus-background pdfs from all categories are also weighted and summed, shown as the solid line.

- This choice of event weight is designed to enhance the contribution of events from categories with higher signal-to-background ratio in a way that approximately matches the impact of these events in the categorized analysis of the data

- Shape description: a double-sided Crystal Ball (DSCB) function， a Gaussian distribution around the peak region, continued by power-law tails at lower and higher *mγγ* values.

H→γγ: Production Mode Cross Sections

[Submitted to JHEP]

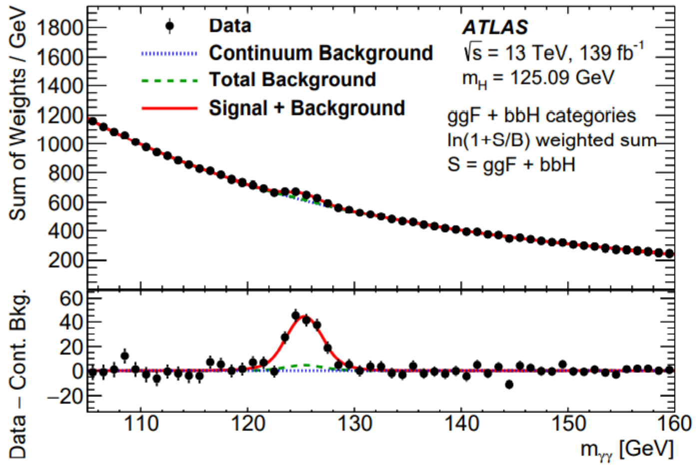

(a) ggF+ $b\bar{b}H$

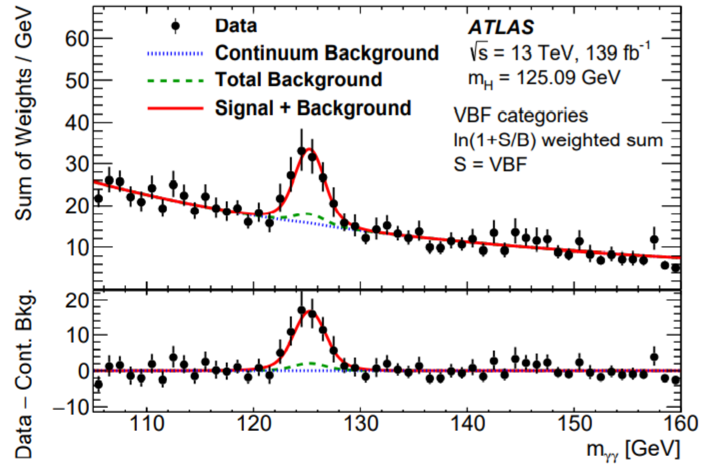

(b) VBF

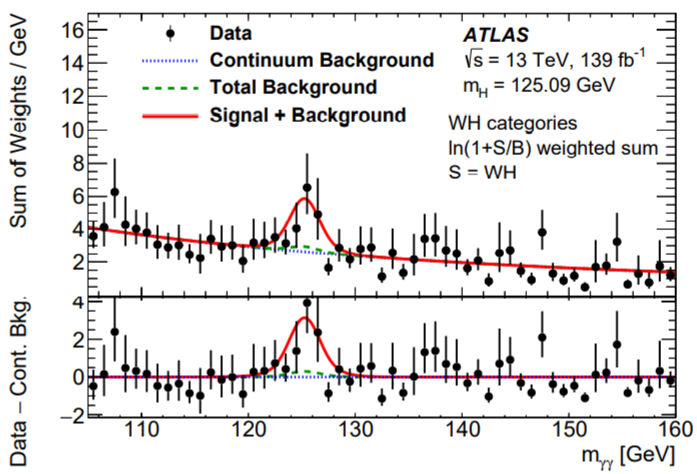

(c) WH

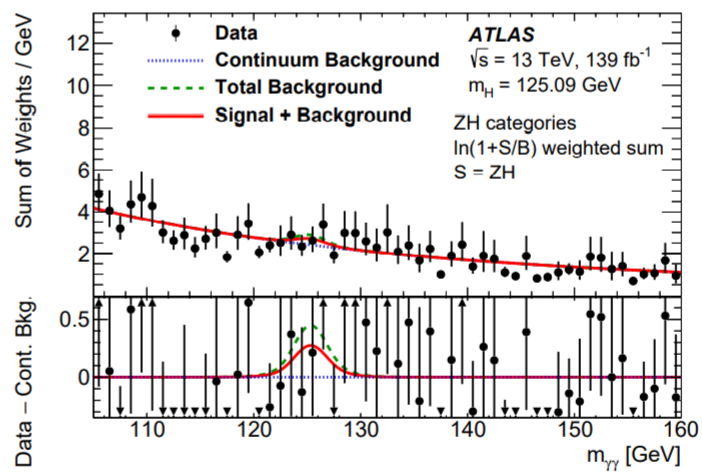

(d) ZH

H→γγ: Production Mode Cross Sections

Submitted to JHEP

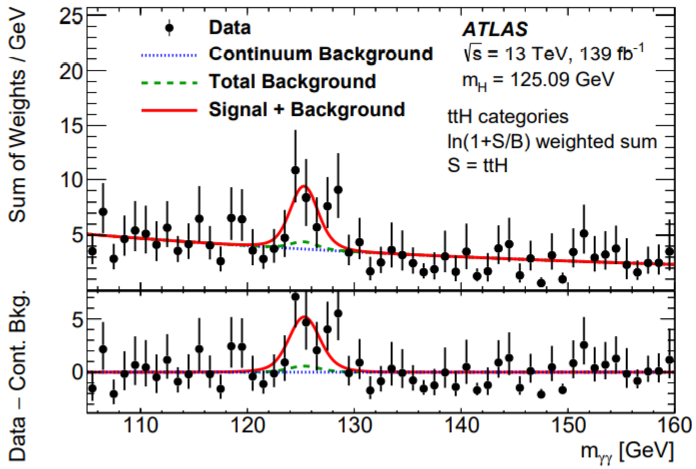

(e) $t\bar{t}H$

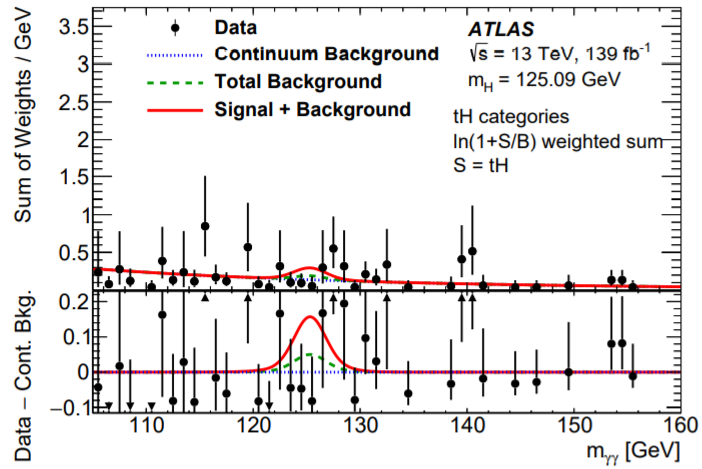

(f) tH

In this calculation, only Higgs boson events from the targeted production processes are considered as signal events.

Higgs boson events from other processes as well as the continuum background events are considered as background.

H→γγ: Production Mode Cross Sections (breakdown)

Uncertainty source	$\Delta\mu$ [%]
Theory uncertainties	
Higher-Order QCD Terms	±3.8
Branching Ratio	±3.0
Underlying Event and Parton Shower	±2.5
PDF and α_s	±2.1
Matrix Element	±1.0
Modeling of Heavy Flavor Jets in non-$t\bar{t}H$ Processes	< ±1
Experimental uncertainties	
Photon energy resolution	±2.8
Photon efficiency	±2.6
Luminosity	±1.8
Pile-up	±1.5
Background modelling	±1.3
Photon energy scale	< ±1
Jet/$E_{\mathrm{T}}^{\mathrm{miss}}$	< ±1
Flavour tagging	< ±1
Leptons	< ±1
Higgs boson mass	< ±1

Submitted to JHEP

Inclusive case

H→γγ: Production Mode XSs

Submitted to JHEP

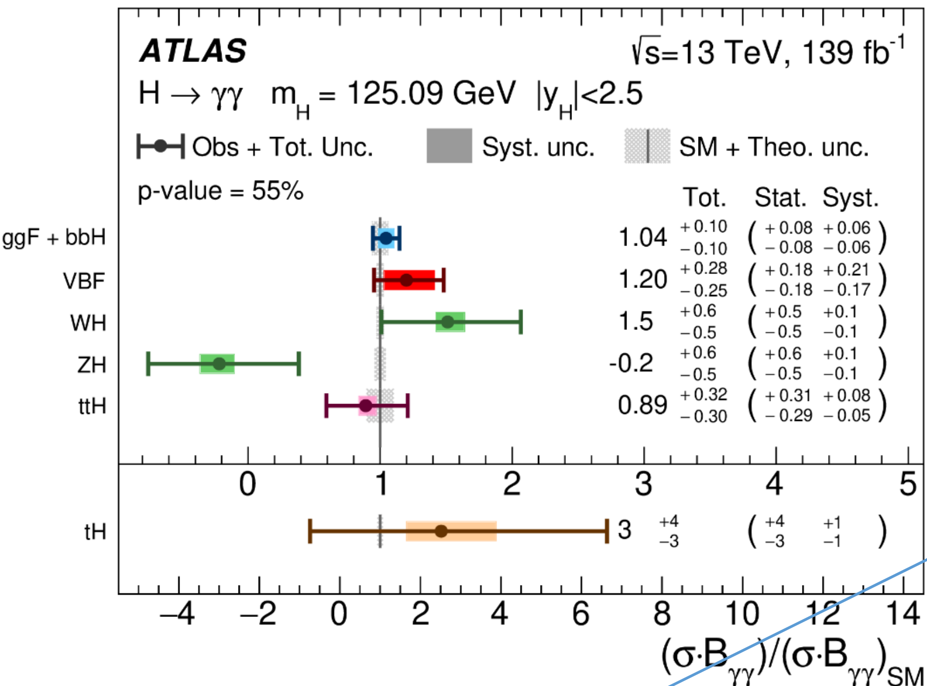

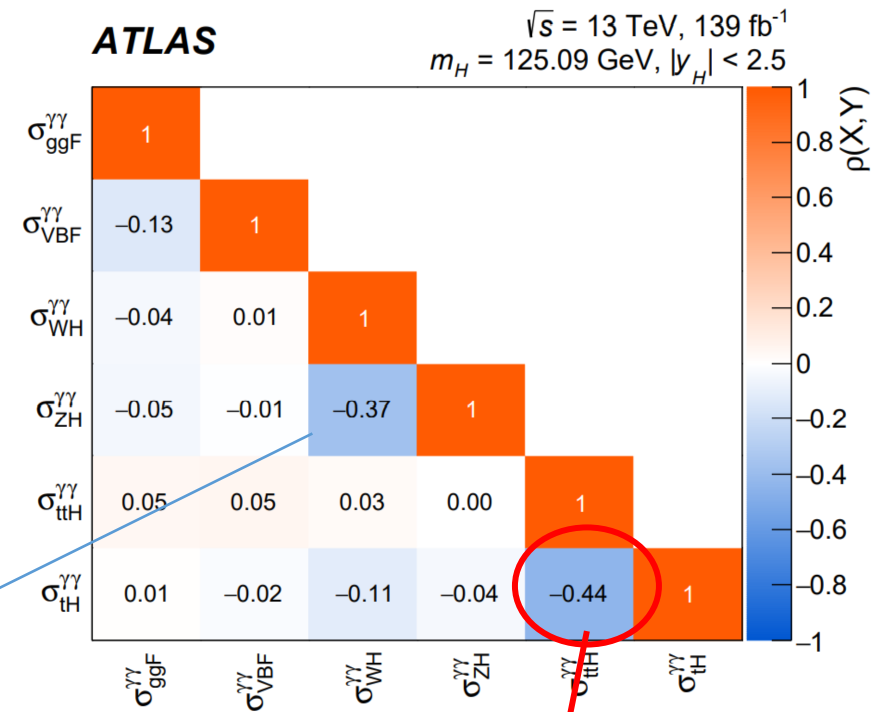

Due to contamination by qq →Hlν events in the categories targeting the pp → $H\nu\bar{\nu}$ process.

Due to the ttH contamination in the categories targeting tH

$H \to \gamma\gamma$: STXS (28 pois)

Submitted to JHEP

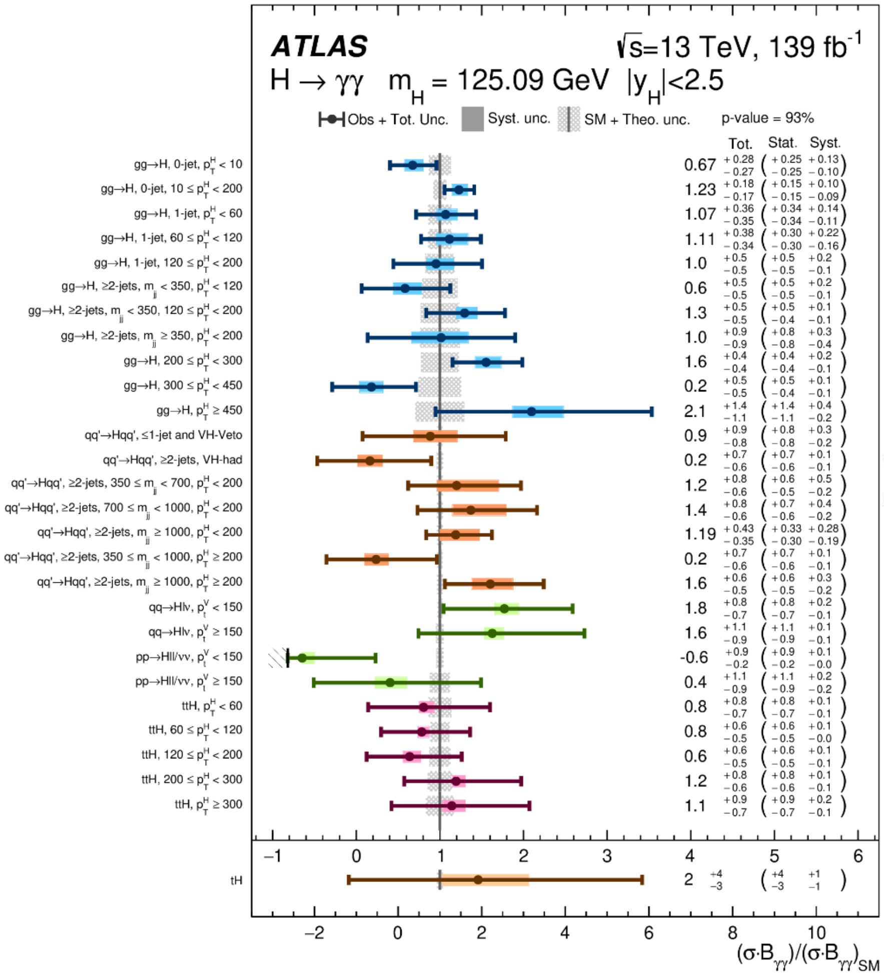

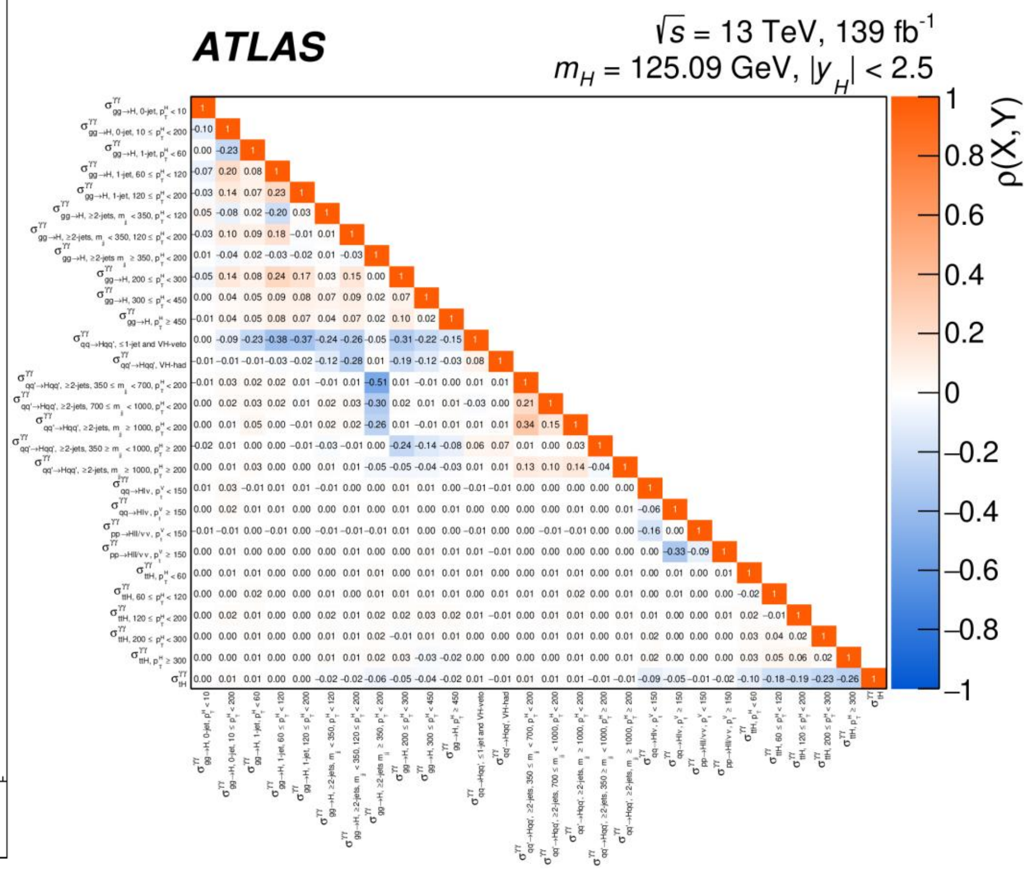

$H \rightarrow \gamma\gamma$: STXS (28 pois)

Table 1: Best-fit values and uncertainties for the production cross-section times $H \rightarrow \gamma\gamma$ branching ratio ($\sigma_i \times B_{\gamma\gamma}$) in each STXS region. The values for the $gg \rightarrow H$ process also include the contributions from $b\bar{b}H$ production. The total uncertainties are decomposed into statistical (Stat.) and systematic (Syst.) uncertainties. The uncertainties for the $pp \rightarrow H\ell\ell/\nu\bar{\nu}$, $p_T^V < 150$ GeV region are truncated at the value for which the model pdf becomes negative. SM predictions are also shown for each quantity with their total uncertainties.

STXS region ($\sigma_i \times B_{\gamma\gamma}$)	Value [fb]	Uncertainty [fb] Total	Stat.	Syst.	SM prediction [fb]
$gg \rightarrow H$, 0-jet, $p_T^H < 10$ GeV	10	$^{+4}_{-4}$	$^{+4}_{-4}$	$^{+2}_{-1}$	15^{+2}_{-2}
$gg \rightarrow H$, 0-jet, $p_T^H \geq 10$ GeV	58	$^{+9}_{-8}$	$^{+7}_{-7}$	$^{+5}_{-4}$	47^{+4}_{-4}
$gg \rightarrow H$, 1-jet, $p_T^H < 60$ GeV	16	$^{+5}_{-5}$	$^{+5}_{-5}$	$^{+2}_{-2}$	15^{+2}_{-2}
$gg \rightarrow H$, 1-jet, $60 \leq p_T^H < 120$ GeV	11	$^{+4}_{-3}$	$^{+3}_{-3}$	$^{+2}_{-2}$	10^{+1}_{-1}
$gg \rightarrow H$, 1-jet, $120 \leq p_T^H < 200$ GeV	1.6	$^{+0.9}_{-0.9}$	$^{+0.9}_{-0.8}$	$^{+0.4}_{-0.2}$	$1.7^{+0.3}_{-0.3}$
$gg \rightarrow H$, $\geq$ 2-jets, $m_{jj} < 350$ GeV, $p_T^H < 120$ GeV	4	$^{+4}_{-3}$	$^{+3}_{-3}$	$^{+1}_{-1}$	7^{+1}_{-1}
$gg \rightarrow H$, $\geq$ 2-jets, $m_{jj} < 350$ GeV, $120 \leq p_T^H < 200$ GeV	2.8	$^{+1.0}_{-1.0}$	$^{+1.0}_{-1.0}$	$^{+0.3}_{-0.2}$	$2.1^{+0.5}_{-0.5}$
$gg \rightarrow H$, $\geq$ 2-jets, $m_{jj} \geq 350$ GeV, $p_T^H < 200$ GeV	2	$^{+2}_{-2}$	$^{+2}_{-2}$	$^{+1}_{-1}$	$2.0^{+0.5}_{-0.5}$
$gg \rightarrow H$, $200 \leq p_T^H < 300$ GeV	1.6	$^{+0.4}_{-0.4}$	$^{+0.4}_{-0.4}$	$^{+0.2}_{-0.1}$	$1.0^{+0.2}_{-0.2}$
$gg \rightarrow H$, $300 \leq p_T^H < 450$ GeV	0.04	$^{+0.13}_{-0.11}$	$^{+0.12}_{-0.11}$	$^{+0.03}_{-0.03}$	$0.24^{+0.06}_{-0.06}$
$gg \rightarrow H$, $p_T^H \geq 450$ GeV	0.09	$^{+0.06}_{-0.05}$	$^{+0.06}_{-0.05}$	$^{+0.02}_{-0.01}$	$0.04^{+0.01}_{-0.01}$
$qq' \rightarrow Hqq'$, $\leq$ 1-jet and VH-veto	6	$^{+6}_{-5}$	$^{+6}_{-5}$	$^{+2}_{-1}$	$6.6^{+0.2}_{-0.2}$
$qq' \rightarrow Hqq'$, VH-had	0.19	$^{+0.85}_{-0.73}$	$^{+0.83}_{-0.71}$	$^{+0.17}_{-0.17}$	$1.16^{+0.04}_{-0.04}$
$qq' \rightarrow Hqq'$, $\geq$ 2-jets, $350 \leq m_{jj} < 700$ GeV, $p_T^H < 200$ GeV	1.5	$^{+0.9}_{-0.7}$	$^{+0.7}_{-0.6}$	$^{+0.6}_{-0.3}$	$1.22^{+0.04}_{-0.04}$
$qq' \rightarrow Hqq'$, $\geq$ 2-jets, $700 \leq m_{jj} < 1000$ GeV, $p_T^H < 200$ GeV	0.8	$^{+0.5}_{-0.4}$	$^{+0.4}_{-0.3}$	$^{+0.2}_{-0.1}$	$0.58^{+0.02}_{-0.02}$
$qq' \rightarrow Hqq'$, $\geq$ 2-jets, $m_{jj} \geq 1000$ GeV, $p_T^H < 200$ GeV	1.2	$^{+0.4}_{-0.4}$	$^{+0.3}_{-0.3}$	$^{+0.3}_{-0.2}$	$1.00^{+0.03}_{-0.03}$
$qq' \rightarrow Hqq'$, $\geq$ 2-jets, $350 \leq m_{jj} < 1000$ GeV, $p_T^H \geq 200$ GeV	0.04	$^{+0.12}_{-0.10}$	$^{+0.12}_{-0.10}$	$^{+0.02}_{-0.02}$	$0.167^{+0.005}_{-0.005}$
$qq' \rightarrow Hqq'$, $\geq$ 2-jets, $m_{jj} \geq 1000$ GeV, $p_T^H \geq 200$ GeV	0.27	$^{+0.11}_{-0.09}$	$^{+0.10}_{-0.08}$	$^{+0.05}_{-0.04}$	$0.166^{+0.005}_{-0.005}$
$qq \rightarrow H\ell\nu$, $p_T^V < 150$ GeV	1.4	$^{+0.6}_{-0.6}$	$^{+0.6}_{-0.6}$	$^{+0.1}_{-0.1}$	$0.79^{+0.02}_{-0.02}$
$qq \rightarrow H\ell\nu$, $p_T^V \geq 150$ GeV	0.20	$^{+0.13}_{-0.11}$	$^{+0.13}_{-0.11}$	$^{+0.02}_{-0.01}$	$0.121^{+0.005}_{-0.005}$
$pp \rightarrow H\ell\ell/\nu\bar{\nu}$, $p_T^V < 150$ GeV	−0.29	$^{+0.40}_{-0.08}$	$^{+0.39}_{-0.08}$	$^{+0.07}_{-0.00}$	$0.45^{+0.02}_{-0.02}$
$pp \rightarrow H\ell\ell/\nu\bar{\nu}$, $p_T^V \geq 150$ GeV	0.04	$^{+0.10}_{-0.08}$	$^{+0.10}_{-0.08}$	$^{+0.02}_{-0.02}$	$0.09^{+0.01}_{-0.01}$
$t\bar{t}H$, $p_T^H < 60$ GeV	0.22	$^{+0.21}_{-0.18}$	$^{+0.21}_{-0.18}$	$^{+0.03}_{-0.01}$	$0.27^{+0.04}_{-0.04}$
$t\bar{t}H$, $60 \leq p_T^H < 120$ GeV	0.32	$^{+0.23}_{-0.20}$	$^{+0.23}_{-0.20}$	$^{+0.04}_{-0.02}$	$0.40^{+0.05}_{-0.05}$
$t\bar{t}H$, $120 \leq p_T^H < 200$ GeV	0.18	$^{+0.18}_{-0.15}$	$^{+0.17}_{-0.15}$	$^{+0.04}_{-0.02}$	$0.29^{+0.04}_{-0.04}$
$t\bar{t}H$, $200 \leq p_T^H < 300$ GeV	0.14	$^{+0.09}_{-0.07}$	$^{+0.09}_{-0.07}$	$^{+0.01}_{-0.01}$	$0.12^{+0.02}_{-0.02}$
$t\bar{t}H$, $p_T^H \geq 300$ GeV	0.06	$^{+0.05}_{-0.04}$	$^{+0.05}_{-0.04}$	$^{+0.01}_{-0.01}$	$0.06^{+0.01}_{-0.01}$
tH	0.4	$^{+0.8}_{-0.6}$	$^{+0.7}_{-0.6}$	$^{+0.2}_{-0.2}$	$0.19^{+0.01}_{-0.02}$

Submitted to JHEP

Results for STXS

$H \to ZZ^* \to 4\ell$: Inclusive and Differential Cross Section

Eur. Phys. J. C 80, 942 (2020)

Matrix-based likelihood unfolding

Higgs boson kinematic-related variables	
$p_T^{4\ell}$, $\lvert y_{4\ell}\rvert$	Transverse momentum and rapidity of the four-lepton system
m_{12}, m_{34}	Invariant mass of the leading and subleading lepton pair
$\lvert \cos\theta^* \rvert$	Magnitude of the cosine of the decay angle of the leading lepton pair in the four-lepton rest frame relative to the beam axis
$\cos\theta_1$, $\cos\theta_2$	Production angles of the anti-leptons from the two Z bosons, where the angle is relative to the Z vector.
ϕ, ϕ_1	Two azimuthal angles between the three planes constructed from the Z bosons and leptons in the Higgs boson rest frame.
Jet-related variables	
N_{jets}, $N_{b\text{-jets}}$	Jet and b-jet multiplicity
$p_T^{\text{lead. jet}}$, $p_T^{\text{sublead. jet}}$	Transverse momentum of the leading and subleading jet, for events with at least one and two jets, respectively. Here, the leading jet refers to the jet with the highest p_T in the event, while subleading refers to the jet with the second-highest p_T.
m_{jj}, $\lvert\Delta\eta_{jj}\rvert$, $\Delta\phi_{jj}$	Invariant mass, difference in pseudorapidity, and signed difference in ϕ of the leading and subleading jets for events with at least two jets
Higgs boson and jet-related variables	
$p_T^{4\ell j}$, $m_{4\ell j}$	Transverse momentum and invariant mass of the four-lepton system and leading jet, for events with at least one jet
$p_T^{4\ell jj}$, $m_{4\ell jj}$	Transverse momentum and invariant mass of the four-lepton system and leading and subleading jets, for events with at least two jets

H→ZZ*→4ℓ: Inclusive and Differential Cross Section

Eur. Phys. J. C 80, 942 (2020)

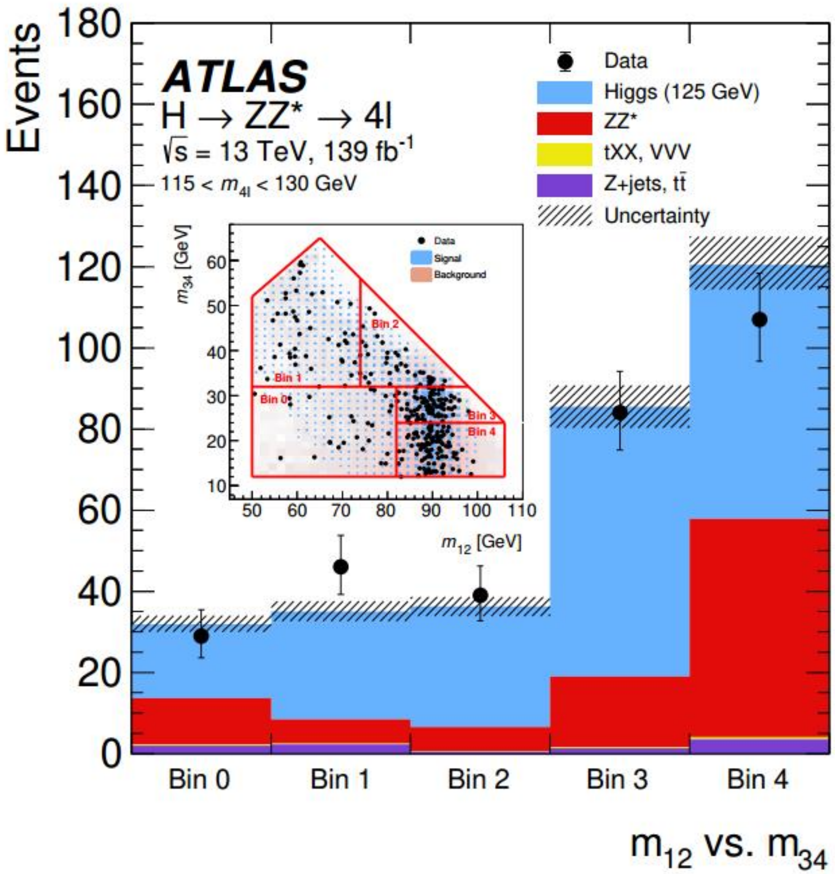

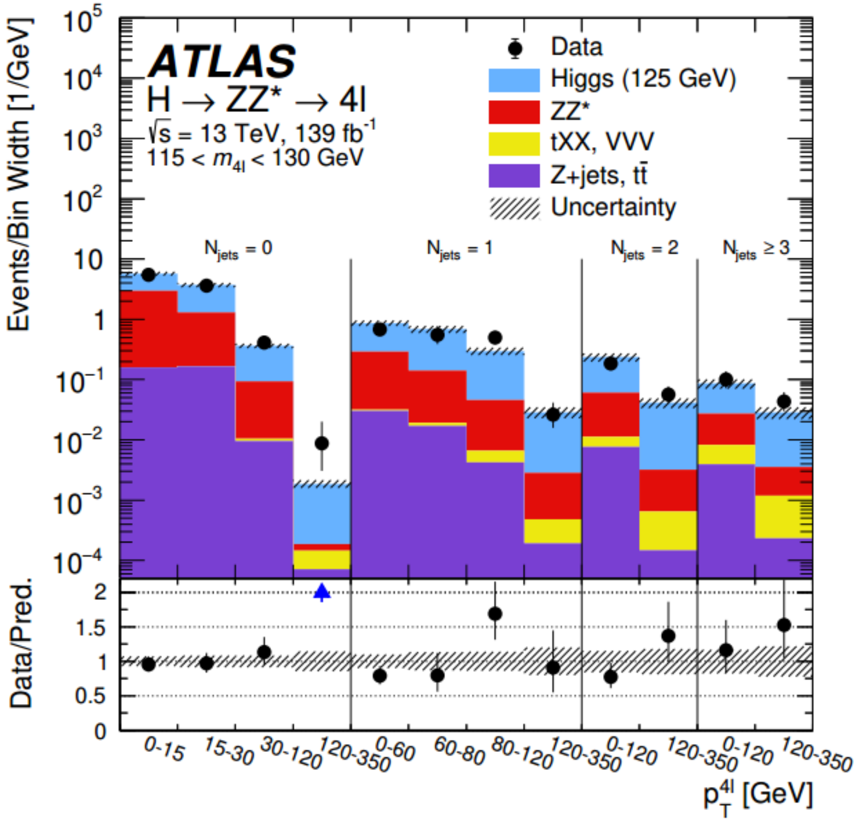

H→ZZ*→4ℓ: Inclusive and Differential Cross Section

Eur. Phys. J. C 80, 942 (2020)

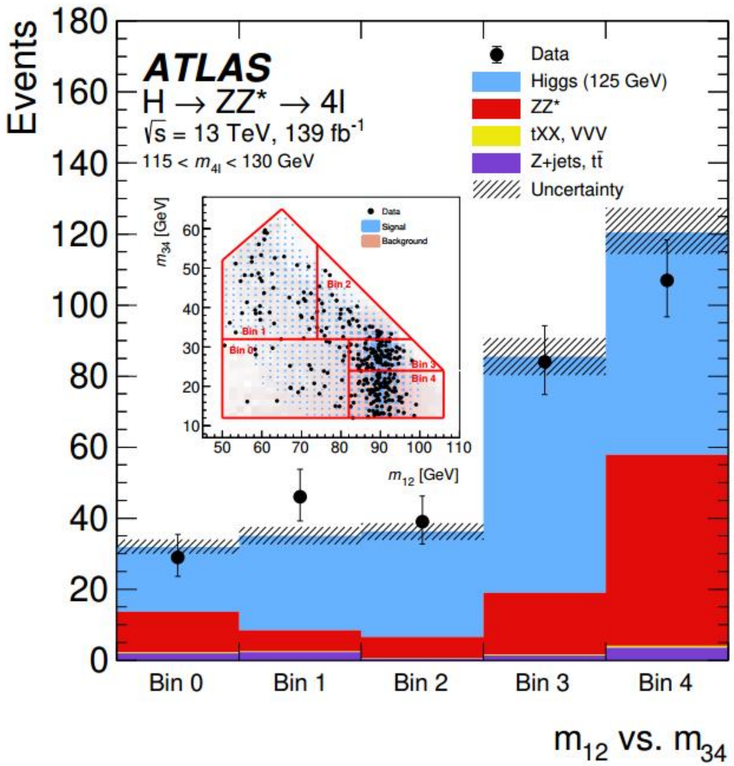

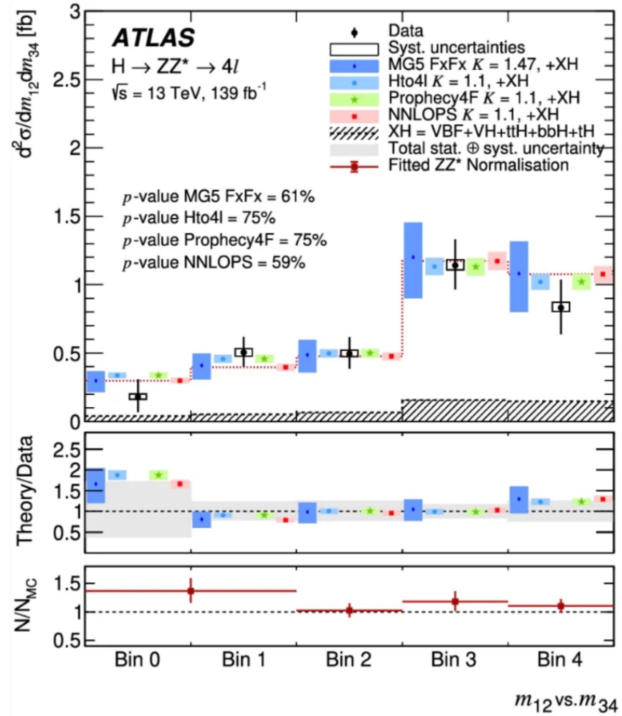

pseudo-observables (arXiv:1504.04018):

ε_L, ε_R : relating the couplings for left- and right-handed leptons to Higgs boson

κ_{ZZ} changes the coupling between H to Z boson

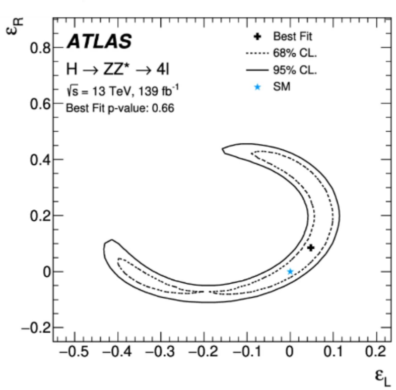

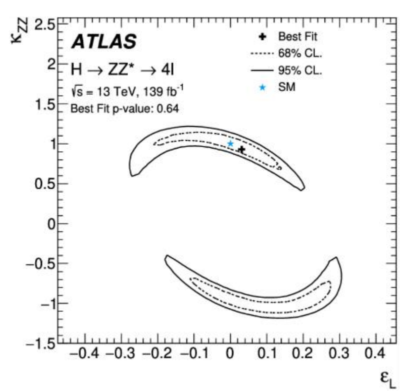

H→ZZ*→4ℓ: Inclusive and Differential Cross Section

[Eur. Phys. J. C 80, 942 (2020)]

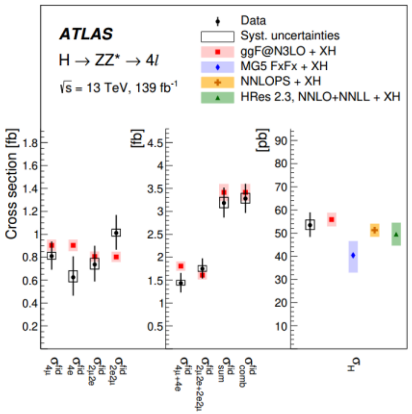

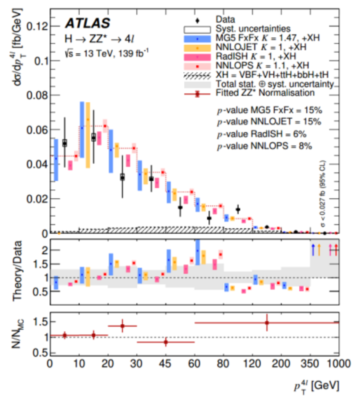

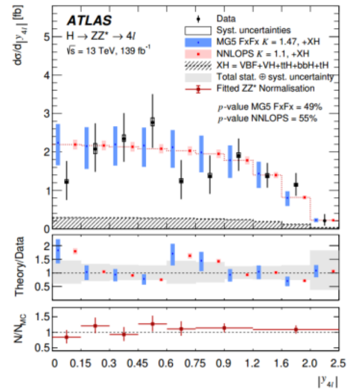

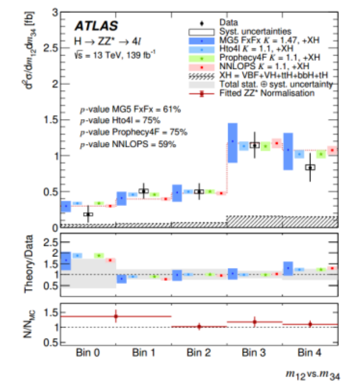

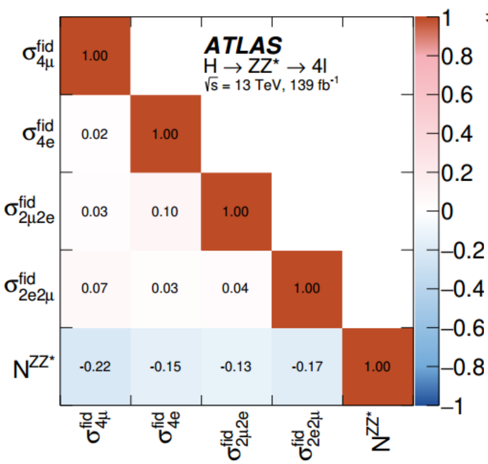

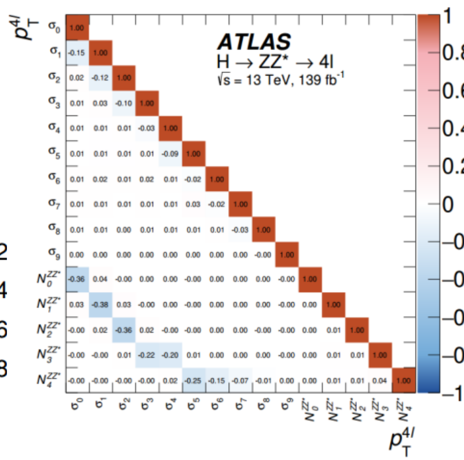

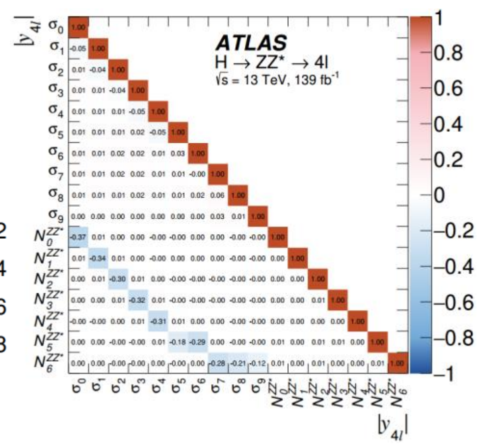

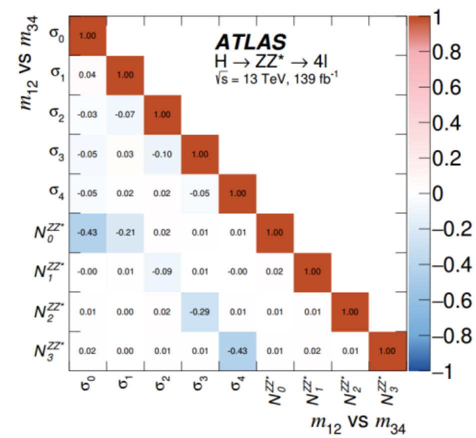

Combination: H(γγ) and H(ZZ)

Submitted to JHEP

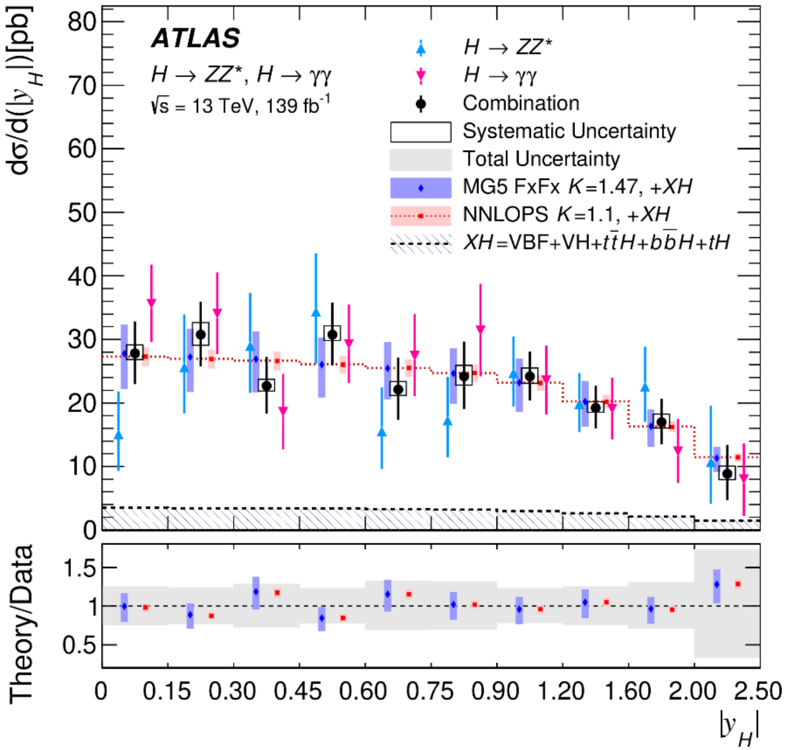

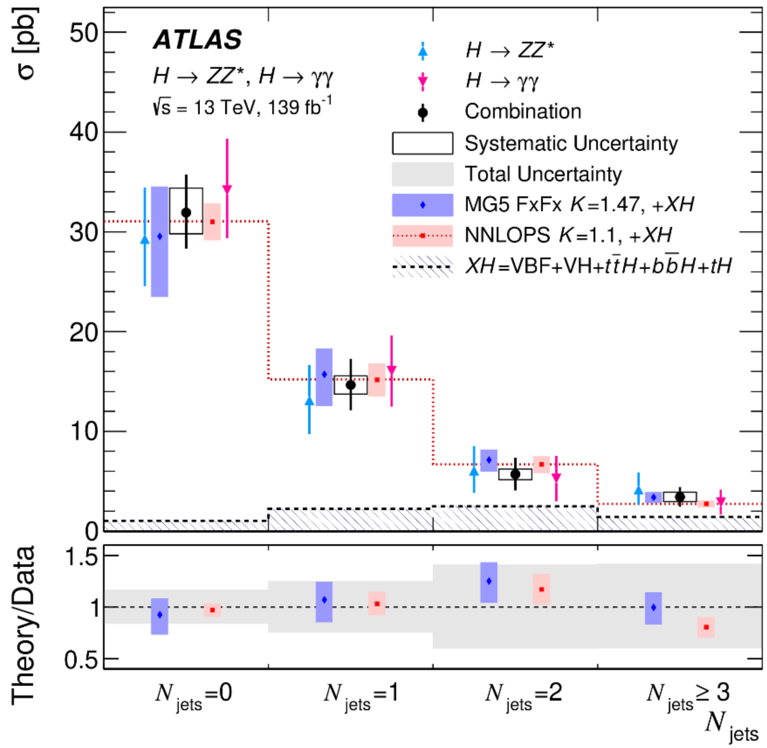

y_H precision: 20-30% up to 2

N_{jets} precision: 20-30%

Probes PDFs and pQCD modeling of the ggF production mechanism

Jet distributions can test pQCD modeling of the ggF production mode, and contributions of other production modes

Combination: H(γγ) and H(ZZ)

[Submitted to JHEP](#)

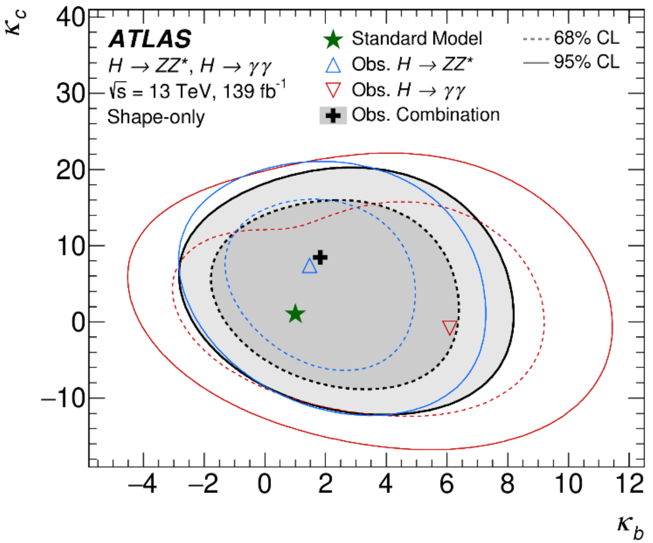

Channel	Parameter	Observed 95% confidence interval	Expected 95% confidence interval
$H \to ZZ^* \to 4\ell$	κ_b	[−1.8, 6.4]	[−3.3, 9.3]
	κ_c	[−7.7, 18.3]	[−12.3, 19.2]
$H \to \gamma\gamma$	κ_b	[−3.5, 10.2]	[−2.5, 8.0]
	κ_c	[−12.6, 18.3]	[−10.1, 17.3]
Combined	κ_b	[−2.0, 7.4]	[−2.0, 7.4]
	κ_c	[−8.6, 17.3]	[−8.5, 15.9]

The results for one coupling modifier are obtained while fixing the other one to the SM expectation

The combined observed limit on k_b less stringent than the individual ZZ* :

- Cross section quadratically depend on k_b
- Double minimum in the NLL scan
- k_b parameter being further from the SM expectation only with the H(γγ) channel

The combined observed limit on k_c similar to the individual ZZ*, but the 68% CL observed combined limits on k_c are worse than the results from the *ZZ* channel :

- The correlation between the k_b and k_c parameters
- Different best-fit k_b observations for ZZ and γγ channel
- Data fluctuations in some p_T^H bins

Interpretation with shape vs. shape + norm.

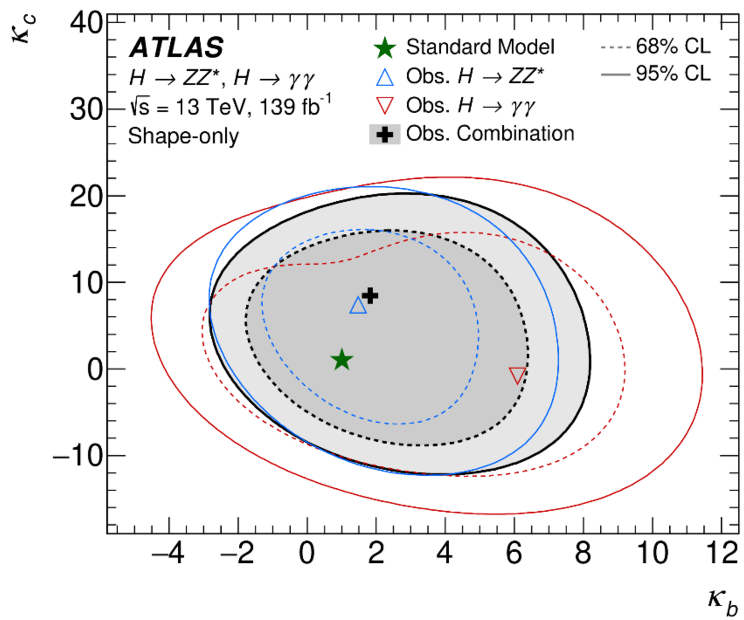

Shape only

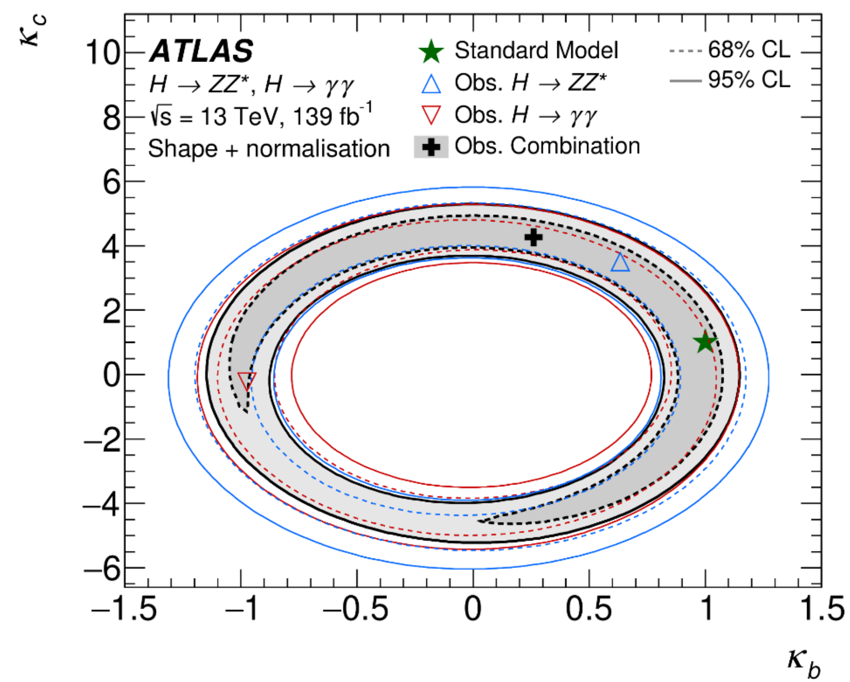

Shape + normalization